



Daniel Josefik, B.Sc.

Preliminary Stability Analysis of the Ingelsberg Rock Slope

Master's Thesis

Submitted in fulfilment of the requirements for the degree of

Diplom-Ingenieur / Diplom-Ingenieurin

Master's programme Geotechnical and Hydraulic Engineering

at

Graz University of Technology

Supervisor

Em.Univ.-Prof. Dipl.-Ing. Dr.mont. Wulf Schubert

Institute of Rock Mechanics and Tunnelling

Graz University of Technology

Supervising Assistants

Andreas Buyer, M.Sc., B.Sc.

Dipl.-Ing. Alexander Kluckner, BSc

Graz, July 2019

EIDESSTATTLICHE ERKLÄRUNG

AFFIDAVIT

Ich erkläre an Eides statt, dass ich die vorliegende Arbeit selbstständig verfasst, andere als die angegebenen Quellen/Hilfsmittel nicht benutzt, und die den benutzten Quellen wörtlich und inhaltlich entnommenen Stellen als solche kenntlich gemacht habe. Das in TUGRAZonline hochgeladene Textdokument ist mit der vorliegenden Masterarbeit identisch.

I declare that I have authored this thesis independently, that I have not used other than the declared sources/resources, and that I have explicitly marked all material which has been quoted either literally or by content from the used sources. The text document uploaded to TUGRAZonline is identical to the present master's thesis.

Datum / Date

Unterschrift / Signature

Abstract

The Ingelsberg rock slope is subjected to frequent detachments of toppling blocks which threaten the surrounding town of Bad Hofgastein. Aim of this thesis is a preliminary numerical study of the slope behaviour. The joint network geometry of the model is based on a digital joint mapping of the detachment area and is implemented as a statistical representation of the joint network. Material and joint parameters were determined by a literature research and their suitability for the toppling mechanism tested by numerical calculations. A numerical 3D Discrete Element Method (DEM) model was set up using the 3DEC software in order to find the most sensitive parameters for failure. Series of sensitivity analyses studying influence mainly of the joint normal and shear stiffness produced possible ranges of properties resulting in the expected behaviour of the rock mass. These results could be used for a further detailed analysis of the slope which would detect presumably failing blocks.

Kurzfassung

Die Hangbewegung am Ingelsberg ist für ihre anhaltende Aktivität bekannt. Immer wieder kippen Felspartien und lösen sich aus dem Felsverband. Diese Felsstürze stellen eine immanente Bedrohung für die darunterliegende Gemeinde Bad Hofgastein dar.

Ziel dieser Masterarbeit ist eine erste numerische Studie über das Böschungsverhalten. Die numerischen Untersuchungen wurden mittels eines 3D-Distinct Element Codes (3DEC, Itasca Consulting Inc.) durchgeführt. Die Trennflächengeometrie wurde anhand einer digitalen Trennflächenkartierung im Ablösebereich bestimmt und als statistische Größe in das Gebirgsmodell implementiert. Die zugrundeliegenden Material- und Trennflächeneigenschaften basieren auf Literaturwerten. Ihr Einfluss auf den Kippmechanismus der Hangbewegung wurde anhand numerischer Sensitivitätsanalysen ermittelt. Hauptfokus der Sensitivitätsanalyse lag dabei auf dem Einfluss der Trennflächennormal- und -schersteifigkeit, um Bereiche zu definieren, welche nachvollziehbar sind und weiterhin zu einem Kippversagen führen. Die gewonnenen Ergebnisse sollen als Grundlage für weitere, detailliertere Untersuchungen hinsichtlich der Böschungstabilität dienen.

Table of contents

1	Introduction	8
1.1	Inducement	8
1.2	Site description.....	10
1.2.1	Geographic setting	10
1.2.2	Geological hydrological setting	11
1.3	Monitoring	14
1.4	Previous studies on the landslide mechanism	17
1.5	State of the art in landslide investigation	20
1.5.1	Digital joint mapping	20
1.5.2	Numerical modelling of slope failures	21
1.6	Objectives	23
2	Methodology	24
2.1	Data basis	24
2.2	Joint network characterisation	25
2.3	Numerical analyses	26
2.3.1	Model geometry.....	27
2.3.2	Global settings	28
2.3.3	Geological units.....	29
	<i>Weak layers</i>	29
	<i>Parallel Joint</i>	32
2.3.4	Material parameters	33
2.3.5	Joint parameters.....	34
	<i>Definition of jkn and jks</i>	36
	<i>ϕ_{joint} sensitivity analysis</i>	38
	<i>Sensitivity analysis jkn and jks</i>	40
3	Results	43
3.1	Joint network characterisation	43
3.2	Numerical analyses	46
3.2.1	Geometry – weak layers.....	46
3.2.2	ϕ_{joint} sensitivity analysis	46
3.2.3	Sensitivity analysis jkn and jks.....	47
4	Discussion	52
4.1	Joint network characterization	52

4.2	Numerical analyses.....	52
4.2.1	Geometry – weak layers.....	52
4.2.2	ϕ_{joint} sensitivity analysis	53
4.2.3	Sensitivity analysis jkn and jks.....	54
5	Conclusion	59
6	Outlook	61
7	References	62
8	Appendix	64

List of figures

Figure 1: Photographs used for photogrammetry; a) impression of the whole active landslide (detachment area = red rectangle, transit zone = orange rectangle and accumulation zone = green rectangle), b) detailed image of the upper detachment area (Wieser et al. 2012).	11
Figure 2: Geological map of the Ingelsberg landslide (Di Matteo et al. 2017); 1 Alluvial deposits; 2 Landslide and talus deposits; 3 Moraine deposits; 4 Black phyllites; 5 Green schist; 6 Calc-mica schist.....	12
Figure 3: Regions of discontinuity mappings (Wilhelmstötter 2013); Left/top sphere diagrams show stereographic projection of all measurements in the region while right/bottom sphere diagrams show average values of the measurements.....	13
Figure 4: Monitoring situation in 2012, modified after Wilhelmstötter (2013); Light blue "F": extensometers, dark blue "G": geodetic points, red "SP": mirror prisms, green: cameras. 15	15
Figure 5: Ingelsberg slope cross section modified after Wilhelmstötter (2013) with description of the monitoring system; 1 Alluvial deposits, 2 Moraine deposits, 3 Black phyllites, 4 Green schist, 5 Calc-mica schist (Di Matteo et al. 2017).....	16
Figure 6: Monitoring data from extensometer nr. 5 and GB-InSAR before and during the event from April 29th (Di Matteo et al. 2017).....	17
Figure 7: Failure mechanism; modified after Wilhelmstötter (2013); the joint sets K1 and K2 lead to the formation of rock towers in the green schist units, which subsequently sink into the underlying weathered weak layers of the calc-mica schists, causing shear displacements and tension forces in the back of the towers as well as their forward rotation and finally toppling.....	18
Figure 8: Base friction model - experiment A (Pichler 2013).....	19
Figure 9: Scaled and referenced 3D surface model of the Ingelsberg rock slope generated with ShapeMetriX3D v4.2 (3GSM GmbH).	25
Figure 10: Approximate position of the medium model within the slope (marked by the white box). Competent rock in the active region is coloured in blue. Red coloured rock mass zones are the weak layers in the active region. The fixed/stable boundary box is coloured in green. Violet and bright blue coloured areas are the competent and weak layers in the "core" region (see section 2.3.3 – "Parallel joint"), respectively.	28
Figure 11: Exemplary 2D cross section through the slope at the Ingelsberg landslide, scale	

1/500, exported from SAGIS online; the red lines indicate lithological boundaries between weak and competent layers (SAGISOnline 2019).	30
Figure 12: Plan view of the surface inclinations, exported from the SAGIS online; Red colour indicates steep regions of the slope, orange and green indicate flatter parts and no colouring (orthophoto) means almost flat surface. Query points with elevation information were used to detect the potential weak layer positions (SAGISOnline 2019).....	31
Figure 13: 2D cross-section through the active landslide derived from the GIS application QGIS (DTM), the elevation is over-scaled by 2:1. The red circle highlights the position of the protective dam.	32
Figure 14: Arrangement of geology with properties, modified after Di Matteo et al. (2017); 1 Alluvial deposits, 2 Moraine deposits, 3 Black phyllites, 4 Green schist, 5 Calc-mica schist.	34
Figure 15: Model regions and joint contacts. Bright blue is a weak layer in the “surface” region, red is a weak layer in the “core” region, dark blue is a competent layer in the “surface” region and green is a competent layer in the “core” region, white bars represent the boundaries (joint contacts) between the single regions.	35
Figure 16: Surface and core regions of the model.....	38
Figure 17: 3DEC model used for the friction angle analysis; the purple zone represents the weak layers, whereas the coloured blocks are the towers of the competent material formed by the intersection of K1 and K2; the yellow zone represents the rigid boundary of the model.	39
Figure 18: 4 movement measurement points for the numerical sensitivity analyses of j_{kn} and j_{ks}	42
Figure 19: Lambert projection of the 2012 model joint sets, the colour of the pole points is set specific and listed in Table 5 The dashed line represents the angle of aperture, whereas the solid line indicates the cone of confidence.	44
Figure 20: Block friction angle analysis showing maximum displacement in the system for a wide range of joint friction angle.....	47
Figure 21: Point 1; movement in Z-direction with series of different j_{kn} values and constant $j_{ks} = 1e3 \text{ Pa/m}$ between blocks.....	48
Figure 22: Movements of point 2 in Z-direction with varying j_{kn} values and a constant $j_{ks} = 1e3 \text{ Pa/m}$ between blocks.....	48
Figure 23: Movement of point 3 in Z-direction with series of different j_{kn} values and constant	

jks = 0 Pa/m between blocks.	49
Figure 24: Movement of point 1 in Z-direction with series of different jkn values and constant jks = 1e3 Pa/m between blocks and weak layer-block contacts.	50
Figure 25: Toppling produced with the parameters jkn = 5e5 Pa/m (“block-block”) and 7.56e6 (“weak layer-block”) and jks = 1e3 Pa/m for both contact types. Capture after 75,000 steps.	50
Figure 26: Evolution of the 4 th sensitivity analysis series. Constant jkn = 1e9 Pa/m, jks = 1e4 Pa/m. The numbers at the upper left part indicate the capture after 100,000 consecutive steps, i.e. 1) after 100,000 steps, 2) after 200,000 steps, etc. Brighter colour is the weak layer and darker the competent layer.	51
Figure 27: Comparison of numerical series with jkn = 2.5e5 Pa/m.	55
Figure 28: Geometry of the full-size model in 3DEC.	61
Figure 29: Foliation - spacing distribution histogram	67
Figure 30: Foliation - trace length distribution histogram	67
Figure 31: K1 - spacing distribution histogram	68
Figure 32: K1 - trace length distribution histogram	68
Figure 33: K2 - spacing distribution histogram	69
Figure 34: K2 - trace length distribution histogram	69
Figure 35: K3 - spacing distribution histogram	70
Figure 36: K3 - trace length distribution histogram	70

List of tables

Table 1: Historical events of Ingelsberg landslide (Wilhelmstötter 2013).....	9
Table 2: Intact rock material properties.....	33
Table 3: Joint parameters.....	36
Table 4: Single steps of numerical calculations with description.....	41
Table 5: Joint set orientations of the mapped discontinuities; DD = Dip Direction, D = Dip angle, CoC = Cone of Confidence, SA = Spherical Aperture, C = Concentration.....	43
Table 6: Geometrical set specifications of the mapped discontinuities in the Head Area; F = frequency, X_s = mean set spacing, X_s = median set spacing, σX_s = spacing standard deviation, TL = mean set trace length, TL = median set trace length, σTL = trace length standard deviation.....	43
Table 7: Absolute differences in the global orientation values of the digitally mapped joint sets (DD_{SMX}/D_{SMX}) and the joint sets according to Wilhelmstötter (2013), given as (DD_W/D_W).....	45
Table 8: Absolute differences in the orientation values in region 5 of the digitally mapped joint sets (DD_{SMX}/D_{SMX}) and the joint sets according to Wilhelmstötter (2013), given as (DD_W/D_W).....	45
Table 9: Absolute differences in the orientation values in region 4 of the digitally mapped joint sets (DD_{SMX}/D_{SMX}) and the joint sets according to Wilhelmstötter (2013), given as (DD_W/D_W).....	45
Table 10: Positions of the weak layers.....	46
Table 11: Numerical series researching jkn in the “block-block” contacts; constant $jks = 1e3 \text{ Pa/m}$ for both contacts: “block-block” and “weak layer-block”.....	57
Table 12: Proposed material parameters.....	58
Table 13: Proposed joint parameters.....	58
Table 14: SAGIS online – elevation of detected weak zones according to sections Active Landslide (1:500 and 1:1000) and Back Slope (1:500, 1:1000); the grey rows highlight the elevations captured in each cross-section.....	64
Table 15: SAGIS online – elevation of the weak zones according to changes in the surface inclination; the grey rows highlight the elevations captured in each cross-section.....	65

Table 16: Weak zones according to DTM in three different cross-sections; the grey rows highlight the elevations captured in each cross-section.....	66
---	----

1 Introduction

The Ingelsberg rock slope is an active landslide located north of Bad Hofgastein, in the southern part of Land Salzburg. First documented rock falls date back to the 18th century. One of the biggest detachments of the rock material took place in 1987, where the detached rock mass is estimated to be 5,000 m³. However, the geological conditions favour detachments of rather small blocks, since the joint sets are almost perpendicular to each other, leading to the formation of towers. Another mechanical feature of the Ingelsberg rock slope is the repeatedly changing sequence of competent and weak layers, causing toppling of the rock towers. Opening of the joints and detachments occur mostly during the spring months, when snowmelt and rain take place. Increased water tables impose water pressure which reduces the effective stresses on joints.

Main aim of this work is a preliminary numerical examination of the Ingelsberg rock slope. The 3D Discrete element method 3DEC v5.2 (Itasca Consulting Group Inc. 2019b) is used to model the slope. Basis for the modelling is previous fieldwork executed in 2012, which produced a 3D model describing the surface and discontinuity systems using a photogrammetry method (chapter 2.2). The resulting joint sets were used to define the joint network in 3DEC. Furthermore, the elevation of the weak layers has been approximated by interpreting changes in the slope inclination (chapter 2.3.3). In the numerical simulations, a series of tests was done in order to estimate the sensitive material parameters of rock and joints sets. The investigation started with a small model with dimensions of several meters to get a rough estimate about the range of the parameters to use and to confirm that the toppling mechanism occurs for the assumed material parameters. After the toppling mechanism was confirmed, the model size was increased and the work proceeded with the sensitivity analyses of the joint stiffness parameters (chapter 2.3.5).

1.1 Inducement

The Ingelsberg area has been known for rock falls for centuries. The oldest documented event dates back to the 18th century, particularly 1774 (Wilhelmstötter 2013). Over the years, many rock falls of different volumes were documented. This illustrates the danger and risk connected to this area as the landslide has been active since observation. In general, rainfall appears to be the main trigger in all major events at Ingelsberg (Wilhelmstötter 2013).

Table 1 sums up the major rock fall events from 1931 to 2012. Major means that police or

authorities were involved to deal with the consequences of the event.

Table 1: Historical events of Ingelsberg landslide (Wilhelmstötter 2013)

Date	Estimated detached mass
July 21, 2012	several hundreds of m ³
December 8, 2011	300 kg block
July 2, 2010	around 1,000 tons
September 8, 2009	10 – 50 m ³
September 23, 2005	no information
2002	several blocks
April 21-22, 2001	several hundreds of m ³
April 23, 2000	no information
Spring 1990	0.5 m ³ block
May 10, 1987	around 5,000 m ³
May 25, 1931	1,500 kg block

As indicated, the event from 1987 was the biggest documented rock fall in the last century. Some of the blocks which detached from the slope stopped in front of the buildings in the valley. One of those blocks was around 30 to 40 m³ and represented a huge risk to buildings and infrastructure. Data indicate that rainfall with cumulated precipitation of more than 120 mm/m² within four days triggered this event (Wilhelmstötter 2013).

1.2 Site description

1.2.1 Geographic setting

The Ingelsberg landslide is situated in the Salzburg province, Austria. More specifically, northeast from the town of Bad Hofgastein in the Gastein valley. The slope is southwest exposed and has an average dip angle of 42° . The toe of the active landslide features an altitude of 1090 m and top of the active landslide features an altitude of 1410 m. The detachment area is approximately 40,000 m² (Di Matteo et al. 2017). The deposit fan length is 80 m (max. 150 m) (SAGISOnline 2019). A rock fall dam has been constructed as a primary rock fall protection for the adjacent infrastructure.

According to Romeo et al. (2014), the Ingelsberg slope can be divided into source area (Head Area), areas of debris accumulation (Middle Bench, Left Talus, Right Talus) and stable rock walls (Upper Wall, Lower Wall), illustrated in Figure 4. Rainfalls and snow repeatedly erode the rock fall debris and accumulate the material along two main channels. Figure 1 shows two of the photographs of the slope which were taken in 2012 from the helicopter and later used for the creation of a 3D surface model. The left image shows an overall area and the active Ingelsberg landslide. It can be easily distinguished between Head Area (source area) at the top of the active landslide and the deposit area with a fan formed by detached material at the toe of the slope. The right image is a detailed photograph of the Head Area from where the rock blocks detach. It can be seen that joint sets form blocks of various volumes and joints are differently opened.

Although located in the temperate climate zone, the location is affected by the humid climate from North-West (Unterberger 2013). Historical records show no increase or a changing trend in the seasonal rainfall. On the contrary, an increase in the mean temperature was recorded over the last 45 years (Wilhelmstötter 2013).

A period of snowmelt, rainfall and additional snowfall preceded the rock fall on April 29, 2013. From April 8, 2013 the air temperature rose significantly causing melting of the whole snow cover. These events resulted in increase of rock movement velocities recorded by both extensometers (from 0.13 mm/day to 1.52 mm/day) and Ground-based Interferometric Synthetic Aperture Radar, GB-InSAR (from 0.46 mm/day to 3.50 mm/day). This phenomenon can be explained by increase of the pore water pressure in the joints and thermal expansion of the rock (Di Matteo et al. 2017).

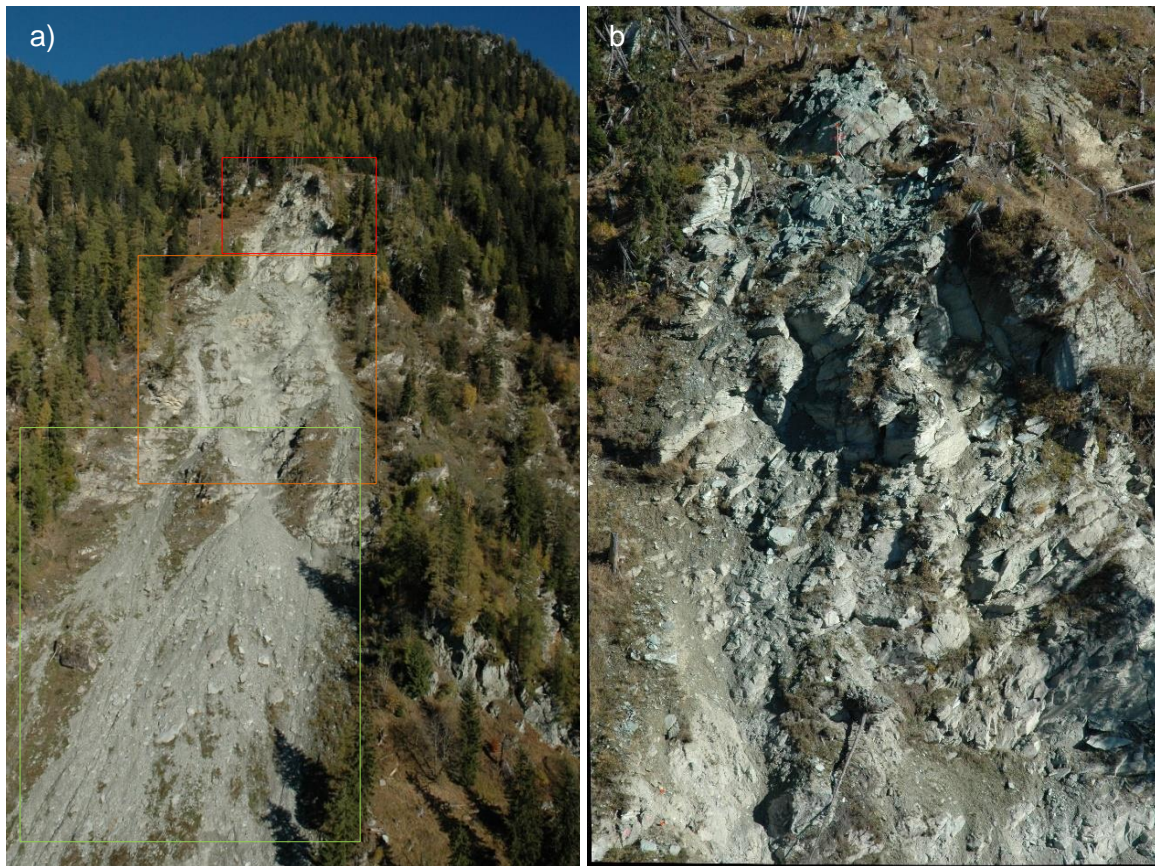


Figure 1: Photographs used for photogrammetry; a) impression of the whole active landslide (detachment area = red rectangle, transit zone = orange rectangle and accumulation zone = green rectangle), b) detailed image of the upper detachment area (Wieser et al. 2012).

1.2.2 Geological hydrological setting

The geology is characterized by the outcropping of metamorphic rocks of the Glockner nappe (Tauern Window) belonging to the Penninic unit. The rock is composed of alternating competent and incompetent lithotypes, later in this thesis called also as “competent” and “weak” layers, which are characterised by different physical and mechanical properties (Di Matteo et al. 2017; Pestal et al. 2009; Schmid et al. 2004).

The foliated rock mass is composed of rather competent green schist, intersected by layers of less competent calc-mica schist (Figure 5). It is important to mention that there is an inconsistency in the geological setting described by various authors (Di Matteo et al. 2017; Pestal et al. 2009; Wilhelmstötter 2013). In this thesis, the nomenclature of Di Matteo et al. (2017) is followed.

The schists overlie competent black phyllites at the slope basement. The black phyllites at the toe are also overlaid by moraine deposits in direction from the slope towards the valley. Furthermore, alluvial deposits are present in the valley in proximity of the Gasteiner Ache. A

geological map is shown in Figure 2. A geological cross-section is given in Figure 5. The orientation of the foliation varies from 335° (region 2) to 35° (region 6) and the dip angles vary from 15° (region 6) to 40° (region 3). Regions of the Ingelsberg rock slope proposed by Wilhelmstötter (2013) are shown in Figure 3. Globally, orientation of the foliation can be described by mean values of 010/25 (Wilhelmstötter 2013).

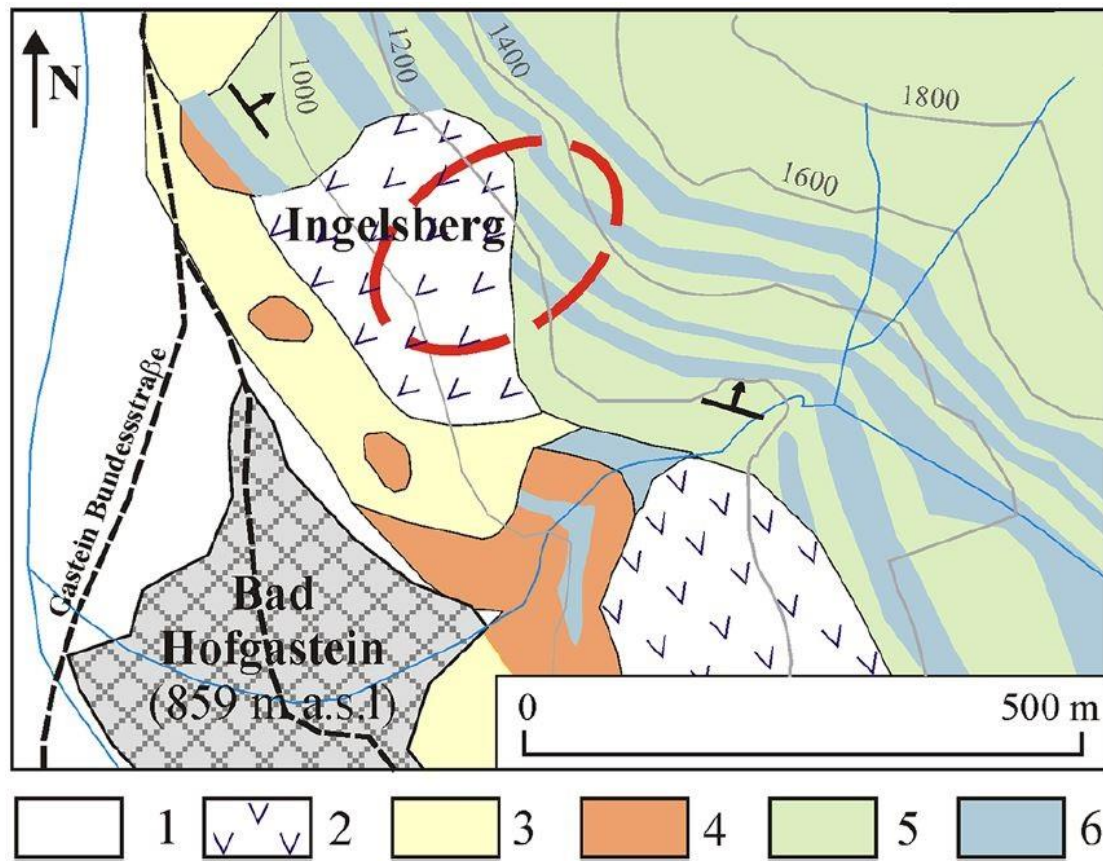


Figure 2: Geological map of the Ingelsberg landslide (Di Matteo et al. 2017); 1 Alluvial deposits; 2 Landslide and talus deposits; 3 Moraine deposits; 4 Black phyllites; 5 Green schist; 6 Calc-mica schist.

In addition to the foliation, two dominant joint sets (K1 and K2) exist. Subordinated, a third joint set of less importance (K3) could be distinguished (Wilhelmstötter 2013). Strike of the joint set K1 has a direction towards North, whereas K2 is usually almost perpendicular to K1. Joint set K3 lies in between K1 and K2. The mean joint set orientations are given with:

- K1 090/85 or 270/85
- K2 015/85 or 200/75
- K3 055/85 or 230/85

The results of the field mapping from Wilhelmstötter (2013) were compared to the digital mapping results from ShapeMetriX3D in section 3.1.

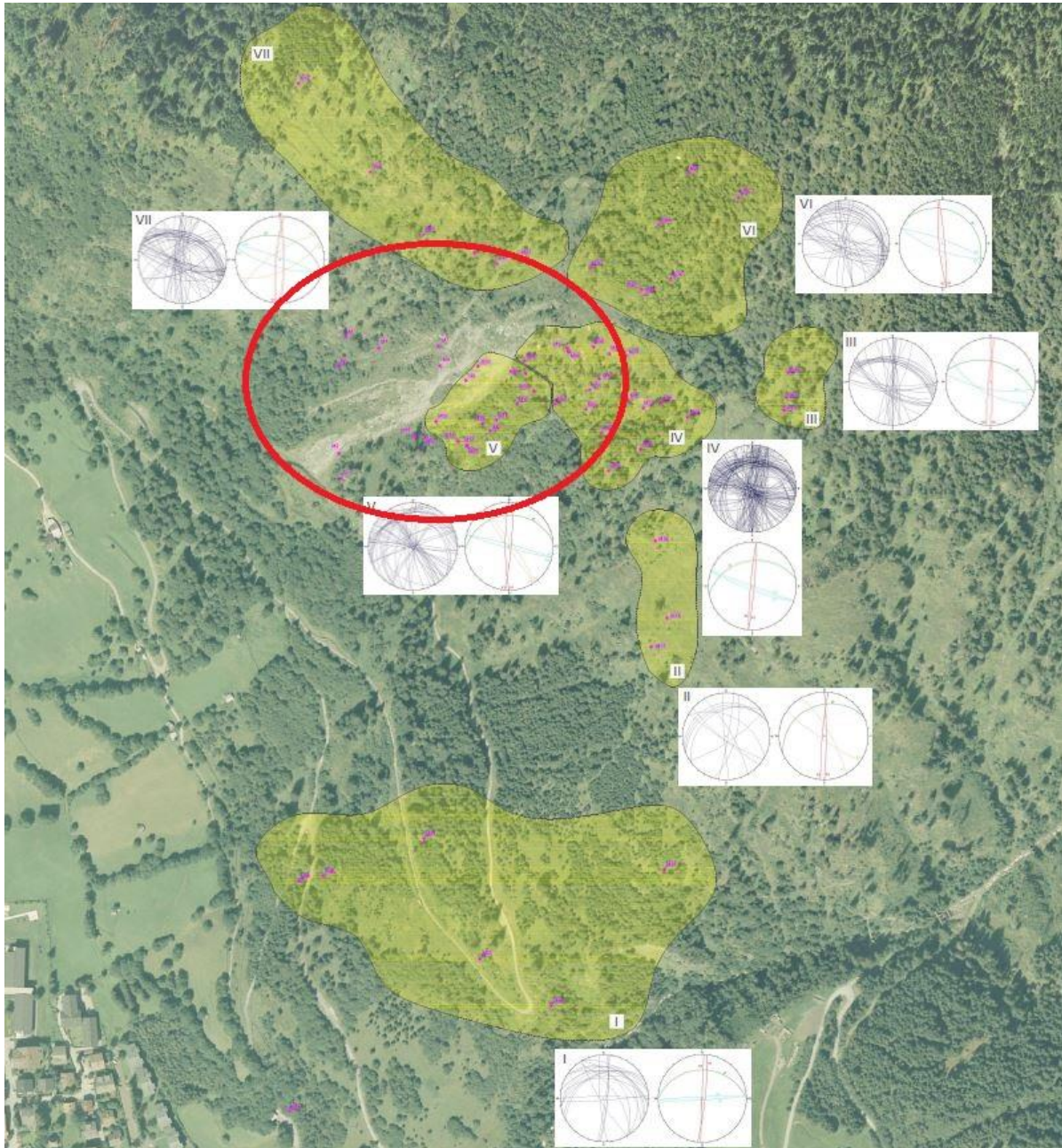


Figure 3: Regions of discontinuity mappings (Wilhelmstötter 2013); Left/top sphere diagrams show stereographic projection of all measurements in the region while right/bottom sphere diagrams show average values of the measurements.

The most significant phenomena observed during the field mapping in 2012 were the aperture and depth of some of the discontinuities. Although it is very hard to determine the actual depth of these open discontinuities, the depth of some of them is estimated to be up to 80 m. Joint openings of up to two meters were observed in the area. These gaps were observed usually in rows with distances between 30 to 80 height meters from each other. It is assumed that these openings are a product of the changing layers of competent and weak material causing tensile stresses in the competent rock mass and later the progression of cracks, forming

blocks, which are later subjected to toppling (Wilhelmstötter 2013). This mechanism is described in chapter 1.4 and Figure 7 in more detail.

Water is undoubtedly one of the crucial features when it comes to rockfalls and general behaviour at the Ingelsberg slope (Wilhelmstötter 2013). Furthermore, erosive forces and weathering must be taken into account apart from the higher water pressures acting on the joint walls as a rainfall consequence.

Since the region is located above 1,000 m above the sea level, snow usually accumulates over the winter. This results into snowmelt in the spring along with higher water pressures and erosion. Additionally, only two small water springs were found in the area. Wilhelmstötter (2013) made a premise that they might be located at the boundary between water-permeable schists and impermeable black phyllites.

1.3 Monitoring

Wilhelmstötter (2013) describes the monitoring system, which was installed in summer of 2012, and evaluates the collected data with regard to the detachments of the rock blocks at the Ingelsberg. There were five extensometers, seven geodetic points, six mirror prisms, three cameras and one thermometer installed in 2012 (Wilhelmstötter 2013). The location of the monitoring devices is shown in Figure 4.

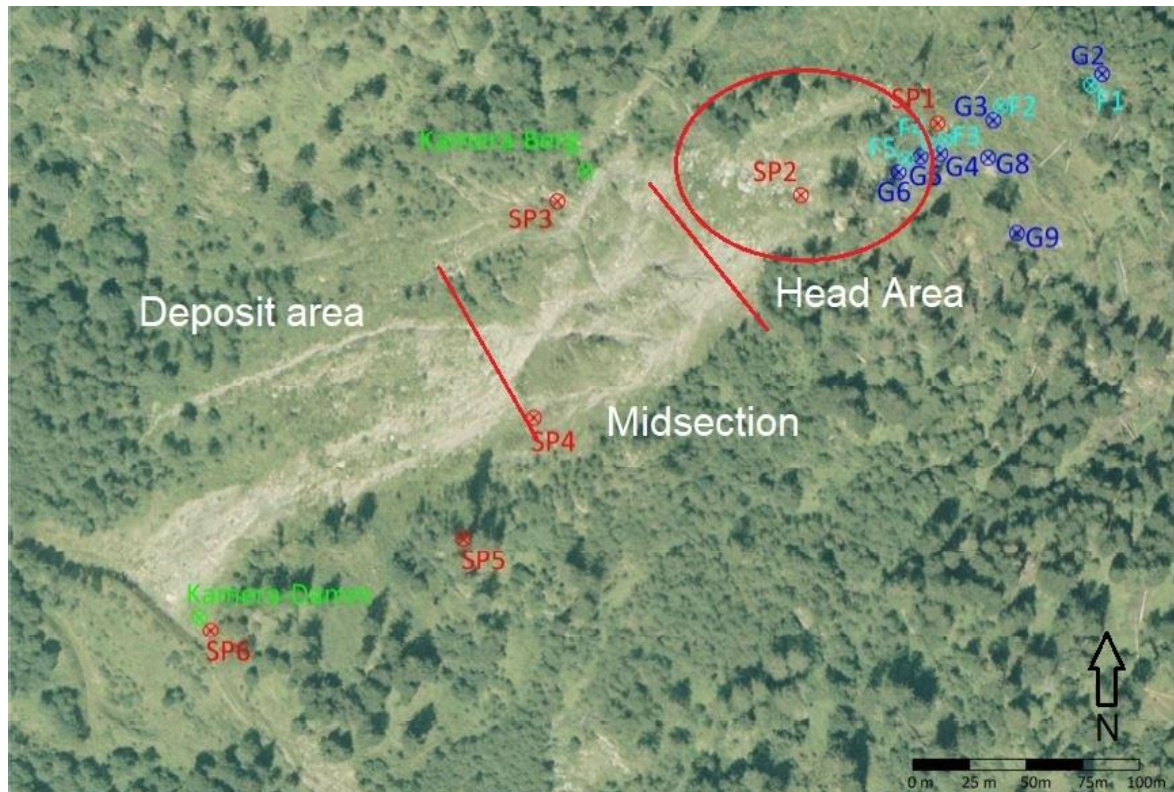


Figure 4: Monitoring situation in 2012, modified after Wilhelmstötter (2013); Light blue "F": extensometers, dark blue "G": geodetic points, red "SP": mirror prisms, green: cameras.

The analysis of the measurement data from extensometers clearly shows a relation between the precipitation and displacements of rock blocks observed by the extensometers. This relationship was observed for the past events as well as for the events during the monitoring and fieldwork period and is expected for future events. Nevertheless, it is very hard to interpret the results precisely since the boundary conditions in the Head Area are constantly changing due to falling blocks, erosion, weathering etc. (Wilhelmstötter 2013). Furthermore, there is no precipitation gauge installed directly at the slope.

Di Matteo et al. (2017) also presents the monitoring system installed in the area of the Ingelsberg landslide and findings collected over the monitoring campaign which took place from March 2013 to July 2014. The work compares various monitoring methods such as surface measurements by newly installed Ground-Based Interferometric Synthetic Aperture Radar (GB-InSAR) or in-depth measurements executed by extensometers installed in the slope, already described by Wilhelmstötter (2013). Combination of such measures allowed a better understanding of the rock mass behaviour. Potential triggering events such as rapid snowmelt or rainfall are taken into account as well. The work focuses mainly on the biggest event of the monitoring campaign which occurred on April 29, 2013. Figure 5 shows a cross section with the geological settings and installed monitoring devices at the Ingelsberg.

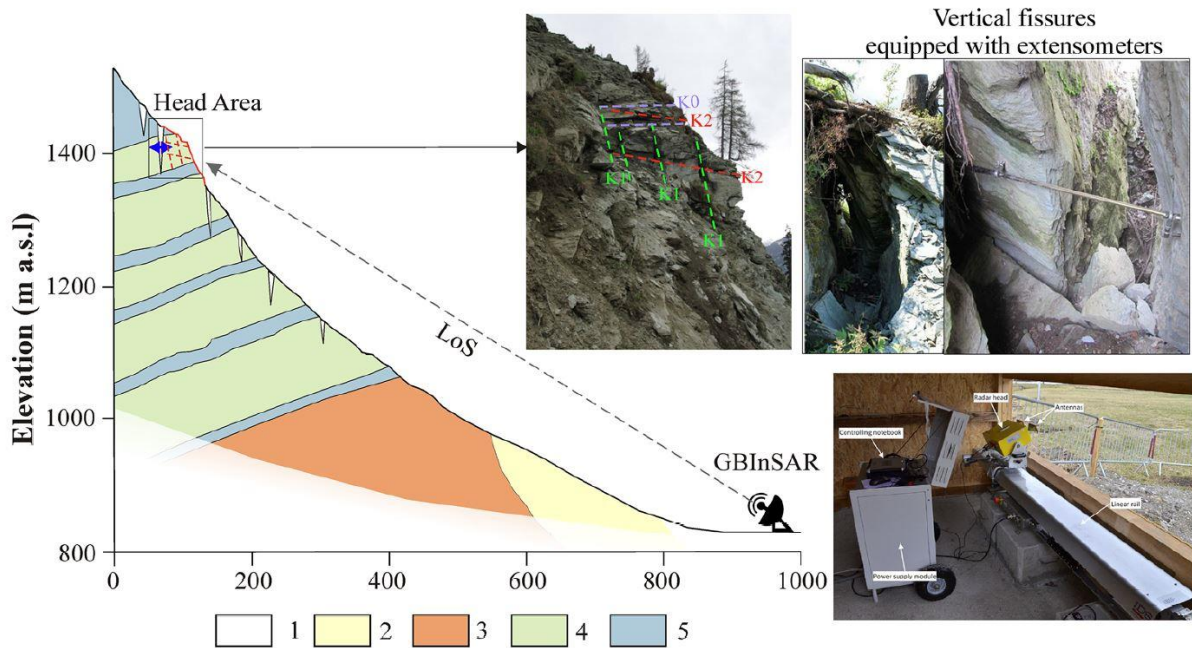


Figure 5: Ingelsberg slope cross section modified after Wilhelmstötter (2013) with description of the monitoring system; 1 Alluvial deposits, 2 Moraine deposits, 3 Black phyllites, 4 Green schist, 5 Calc-mica schist (Di Matteo et al. 2017).

On April 29th, 2013 a rock fall event occurred with a detachment volume of approximately 20 to 40 m³. Data from both InSAR and extensometer nr. 5 (placed at the bottom of the main fracture located 10 meters behind the Head Area) show progressive displacements of the Head Area after April 10, 2013 (Figure 6). The rock mass had moved producing velocities ranging from 0.13 mm/day to 1.52 mm/day for the extensometer and velocities ranging from 0.46 mm/day to 3.50 mm/day detected by the GB-InSAR (Di Matteo et al. 2017).

Due to the ongoing movements and continuing risk for the commune Bad Hofgastein, the slope is still under permanent observation, including the evaluation of the installed geodetical measurement devices as well as onsite inspections by the Geological Survey Salzburg and the clearing of the protection dam at the slope toe.

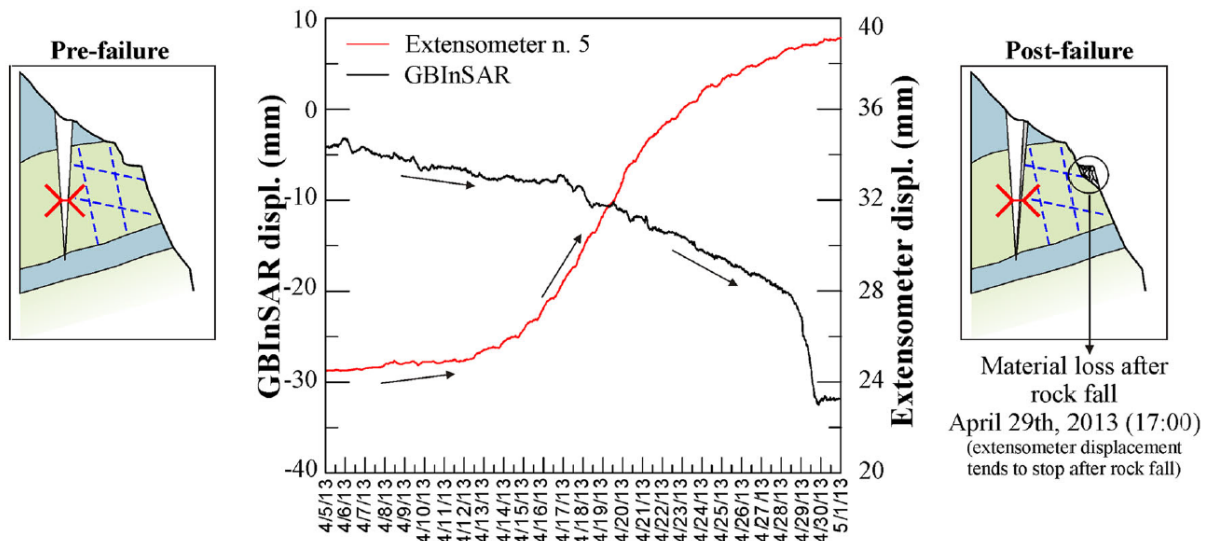


Figure 6: Monitoring data from extensometer nr. 5 and GB-InSAR before and during the event from April 29th (Di Matteo et al. 2017).

1.4 Previous studies on the landslide mechanism

The first documented rock fall event is according to Wilhelmstötter (2013) from 1774, which suggests that inhabitants of Bad Hofgastein have been concerned with possible damages and risks for centuries. There are three main previous studies, which form the basis of this thesis and are crucial source of information for modelling of the slope movement. The first is a digital surface model from 2012, which describes the surface of Ingelsberg by means of an aerial photogrammetry and delivers information about the joint network geometry.

Second is a master's thesis written in 2013 by Franz Wilhelmstötter at the Institute of Soil Mechanics, Foundation Engineering and Computational Geotechnics at TU Graz. This work comprehensively describes the Ingelsberg rock slope and its history, geology, and protective measures. Part of the master's thesis was fieldwork done in summer 2012 as well as the results of a base friction test of the possible failure mechanism according to the mechanical properties of lithotypes (Pichler 2013).

The third work is written by Di Matteo et al. (2017) and describes the monitoring system installed at Ingelsberg comprising mainly of InSAR and extensometers. Its second part deals with the analysis of the monitoring data with regard to a rock fall event that occurred in April 2013.

The geology, namely the structure of the rock mass in combination with the weak layers, is the most important feature, influencing the behaviour of the Ingelsberg slope. Changing layers of the competent and weak rock mass are causing additional tensile stresses in the rock which cause cracking of the rock and opening of the existing joints belonging to the joint system K1.

These openings form so-called rock towers which are subjected to toppling mechanism caused by squeezing of the weak layers. Joint set K2 is perpendicular to K1 and therefore perpendicular to the overall slope dipping (Wilhelmstötter 2013).

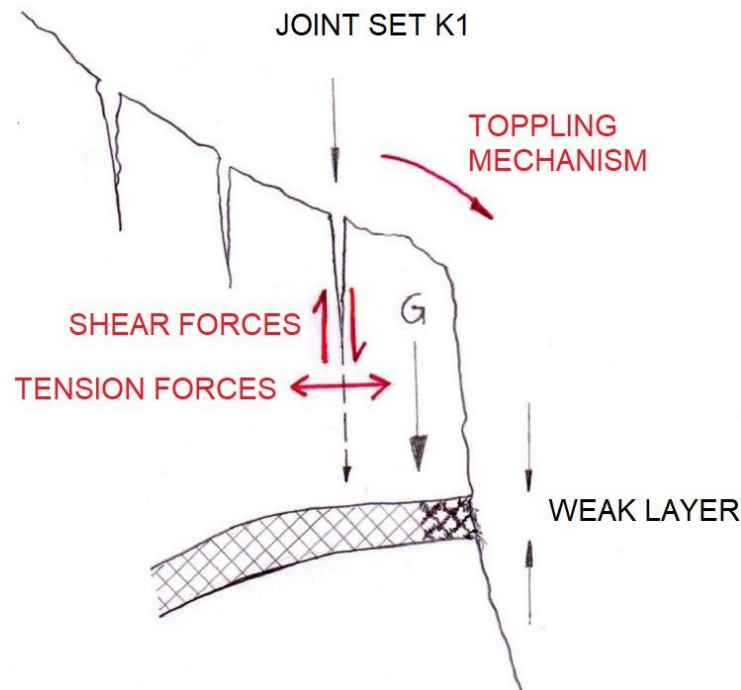


Figure 7: Failure mechanism; modified after Wilhelmstötter (2013); the joint sets K1 and K2 lead to the formation of rock towers in the green schist units, which subsequently sink into the underlying weathered weak layers of the calc-mica schists, causing shear displacements and tension forces in the back of the towers as well as their forward rotation and finally toppling.

In addition to the master's thesis of Wilhelmstötter (2013), a master project with a scaled base friction model was carried out (Pichler 2013). The project focused on the investigation of the failure mechanism of the landslides in the Gasteiner Valley. One part of the project approximated the structural conditions of the Ingelsberg slope as realistically as possible: joint set K1 was modelled with dip angle of $90 \pm 10^\circ$. The schistosity dips with 10° to 35° . The evolution of the experiment is shown in Figure 8. Hard layers were simulated by wooden blocks (bright segments in Figure 8), the weak layers were modelled with a mixture of sand, flour and oil (dark layers in Figure 8). The experiment basically showed the anticipated behaviour: Opening of the joints, forming of the rock "towers" which are subjected to toppling and accumulation of the material at the toe.

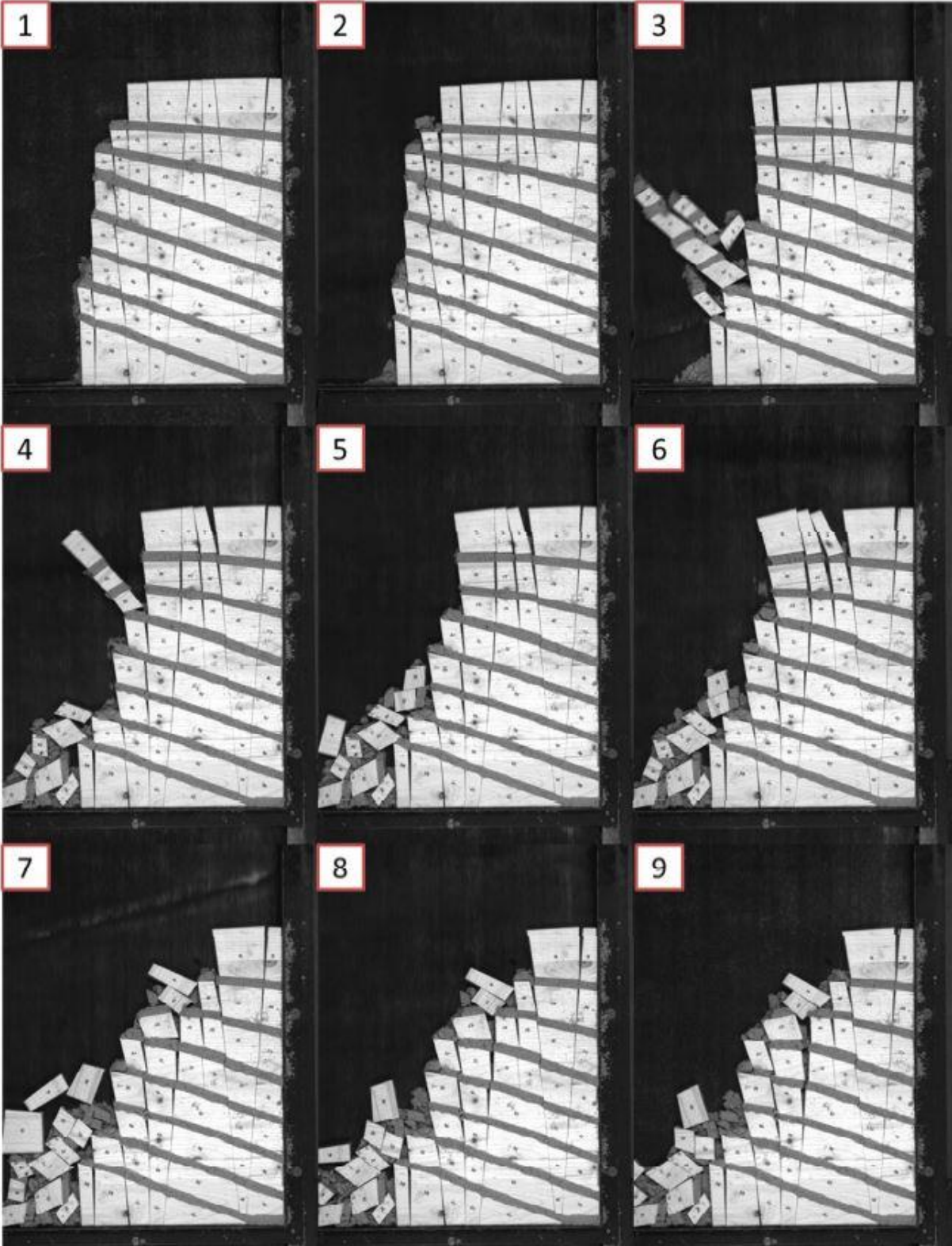


Figure 8: Base friction model - experiment A (Pichler 2013).

1.5 State of the art in landslide investigation

Following chapters describe current state of the art in the field of geotechnical engineering and rock mechanics. These two branches – digital joint mapping and numerical modelling of slope failures – are the most important features for this master's thesis.

1.5.1 Digital joint mapping

Digital joint mapping represents a big step forward in the engineering geology. Engineers and geologists must no longer access the risky areas, which are potentially unstable. Mapping of the rock mass structure features, such as orientation (dip and dip direction), persistence, spacing and block volumes, is necessary for a future analysis of the rock mass behaviour. Modern methods of engineering geology allow users to study the areas of interest from remote and thus safe locations.

3D photogrammetry is nowadays the most common tool for a digital reconstruction of a rock fabric in projects such as rock slopes, benches or tunnel faces. It has been successfully used in many projects (Gaich et al. 2017; Lambert et al. 2012; Sturzenegger and Stead 2009) worldwide.

An even more promising and rapidly developing field is an aerial photogrammetry. Few years ago, it was state of the art to use airplane or helicopter to acquire photographs, suitable for the photogrammetry. This method was flexible and allowed engineers to study a desired area from longer distances and many angles. However, this method has high demands on both finances and man-power. Another big step came with a growth of Unmanned Aerial Vehicle (UAV) technology which allows much more efficient way to obtain images for the aerial photogrammetry. Application of the Structure-from-Motion (SfM) methodology produces surface models of large areas with high resolution in relatively short time. According to Zekkos et al. (2018) the SfM models have comparable accuracy to other surveying techniques such as LiDAR. The biggest advantage of this technology is safe and fast acquisition of data in areas which are inaccessible or unsafe. This helps long-term monitoring since the data can be collected and evaluated more frequently compared to other methods.

Obtained data can be easily and fast processed thanks to the modern software packages such as ShapeMetriX3D or Sirovision which make the joint mapping user friendly and easy to use (Bonilla-Sierra et al. 2015; Gaich et al. 2017). Programmes analyse series of images (two or more) which should have significant overlap and create a 3D surface model of the studied area which can be easily geo-referenced. Software is able to automatically detect the discontinuities, their orientation, persistence, spacing and even make statistical evaluations of mean values, median values and deviations. However, user is still able to control features such

as number of joint sets and must be aware that the program is not completely independent. User must verify the result made by software and e.g. trace the joints manually.

1.5.2 Numerical modelling of slope failures

Slope failures are a very complex and challenging part of the geotechnical engineering. Even though the computational software packages are rapidly developing and are able to calculate very complicated projects, the resulting problem is the degree of simplification and relationship between reality and interpreted model. Slope failures cover a wide range of geotechnical challenges and solver of such problems must always pay attention to clearly interpret the task. There are many software packages computing geotechnical problems using numerical methods. First of them is Finite Element Method (FEM) which is suitable for computation of stability problems of rather homogeneous bodies (continuum) composed of soil or rock layers. Software packages based on FEM usually provide a wide range of constitutive models from simple ones such as Linear elastic or Mohr-Coulomb to complex ones like Hardening soil model (HS) (Itasca Consulting Group Inc. 2019c; Plaxis BV 2019). As already mentioned, these methods are suitable to estimate deformations or overall stability of slopes. Strength reduction method is a main tool to assess the stability of a slope and parameters at which the slope gets unstable (Jing 2003; Pariseau 2012).

On the other hand, when the slope behaviour is expected to be controlled rather by the discontinuities, Distinct Element Method (DEM) is more suitable. The discontinuous material is represented as an assemblage of discrete blocks. The discontinuities are treated as boundary conditions between blocks. Large displacements along the discontinuities and rotations of the blocks are allowed. Individual blocks behave (based on the used constitutive models) as either rigid or deformable material (Itasca Consulting Group Inc. 2019a).

DEM became state of the art for the stability analysis of rock slopes comprising of jointed material and is nowadays used also for assessment of a progressive failure process occurring in the rock mass. Bonilla-Sierra et al. (2015) propose a solution for an unstable rock block located in French Alps using a specially enhanced DEM code for modelling of pre-fractured rock masses. 3D stability analysis studied a rock bridge in a rock and its progressing shear-tensile failure of the intact rock leading to generation of new failure surfaces. Non-persistent fracture planes were implemented in Discrete Fracture Network (DFN). It is important to mention that in this case a Particle Flow Code was used to model single particles which are glued together by cohesive bonds to study the progressive failure between the particles of an intact rock. This resulted into creation of more than 10^6 distinct elements. In general, the whole blocks are usually modelled as one intact piece when assessing the rock behaviour. Tensile and shear strength reduction method was used to evaluate the progressive behaviour.

Calvetti et al. (2018) describe a back analysis of a case history (rock slide) using the DEM code 3DEC. In this case, reliable information about the geo-mechanical and rock mass structure (joint sets) is available. The topography of the slope is obtained with help of material properties evolution, namely continuous reduction of the joint cohesion and tensile strength, i.e. the model starts as a regular jointed block and the slope surface geometry similar to the reality is reached by progressive failures of blocks. Thanks to a very low stress states on the rock slope surface a simple rigid block approach can be used because deformation of the blocks is negligible and not of interest. Unlike in Bonilla-Sierra et al. (2015), the joints are modelled persistent to avoid interlocking in the rock mass. The existence of rock bridges is considered by weighting a rock resistance on the basis of the actual joint persistence, as described by the following theoretical formula (Jennings 1970):

$$c_j = c_r(1 - k); t_j = t_r(1 - k)$$

Where k is the joint persistence, c_j and t_j are the joint cohesion and tensile strength, and c_r and t_r are the same parameters referred to intact rock (Calvetti et al. 2018). Joint cohesion and tensile strength are then reduced until the failure occurs and slope topography similar to the real topography is obtained.

Vanneschi et al. (2019) describe a case study of an open pit environment with the application of 3DEC v5.2 (Itasca Consulting Group Inc. 2019b) for the stability analysis. The case study focuses on toppling behaviour of a blocky rock mass which forms a bench in Melbur Pit located in United Kingdom. Apart from sensitivity analyses on parameters such as friction angle, discontinuity shear and normal stiffness, authors considered also different spacings and orientations of the discontinuities. Unlike in this thesis, the toppling mechanism in Melbur Pit is triggered by the orientation of the discontinuities which form blocks whose centre of gravity acts out of the base of the block. This results into a moment acting on the whole block. Thanks to this mechanism and low stress states at the surface, simpler rigid block modelling can be used in this case as well.

Bonilla-Sierra et al. (2015), Calvetti et al. (2018) and Vanneschi et al. (2019) are just few of the papers dealing with DEM simulations. Nevertheless, they describe the general state of the art of numerical slope modelling used by many other authors.

1.6 Objectives

Generally, the main objective of this master's thesis is the application of state of the art techniques for a preliminary numerical study of the Ingelsberg rock slope based on the studies which were already made and which stated assumptions about the failure mechanism, such as 2012 Model, Wilhelmstötter (2013) and Di Matteo et al. (2017). In particular, the stability of the rock slope should be numerically tested with 3DEC based on the results of a digital joint mapping in the detachment area. The main objective of the numerical analysis is to determine the discontinuity stiffness parameters and to simulate the toppling behaviour of the actual slope. This preliminary study can be used later for further investigations with the inclusion of the water pressure or discrete fracture network (instead of statistical representation of the joint network geometry).

The elaboration of the preliminary study is guided by the following questions:

- What is the joint network geometry in the detachment area and where are the weak layers located?
- What material and joint properties can be obtained from the literature? Will they result in toppling of the blocks in the 3DEC model?
- What are the most sensitive parameters controlling the magnitude and occurrence of the failure mechanism?

2 Methodology

2.1 Data basis

One of the most important sources of information for this master's thesis is a digital surface model (DSM) generated from the digital images of the rock slope made in 2012. This model was created by the Institute for Rock Mechanics and Tunnelling at Graz University of Technology using the SfM application MultiPhoto (v.3.0) of ShapeMetriX3D. The images from the field work were shot from a helicopter. The model is scaled, referenced and north-corrected.

Figure 9 shows the complete 3D model of Ingelsberg landslide created by ShapeMetriX3D. The model is composed totally of 24 sub-images and consists of almost 3 Mio 3D points, which cover a total surface area of 101,042.3 m². This means an average geometric image resolution of 0.04 meter/pixel. The average 3D point spacing is 0.19 meter. Total image size is 64.2 megapixel. The average distance from camera to model ranges from 158 m up to 1,203 m. Photographs were taken by a calibrated camera Nikon D70s with 18 mm focal length. The image resolution is 2000 x 3008 pixel.

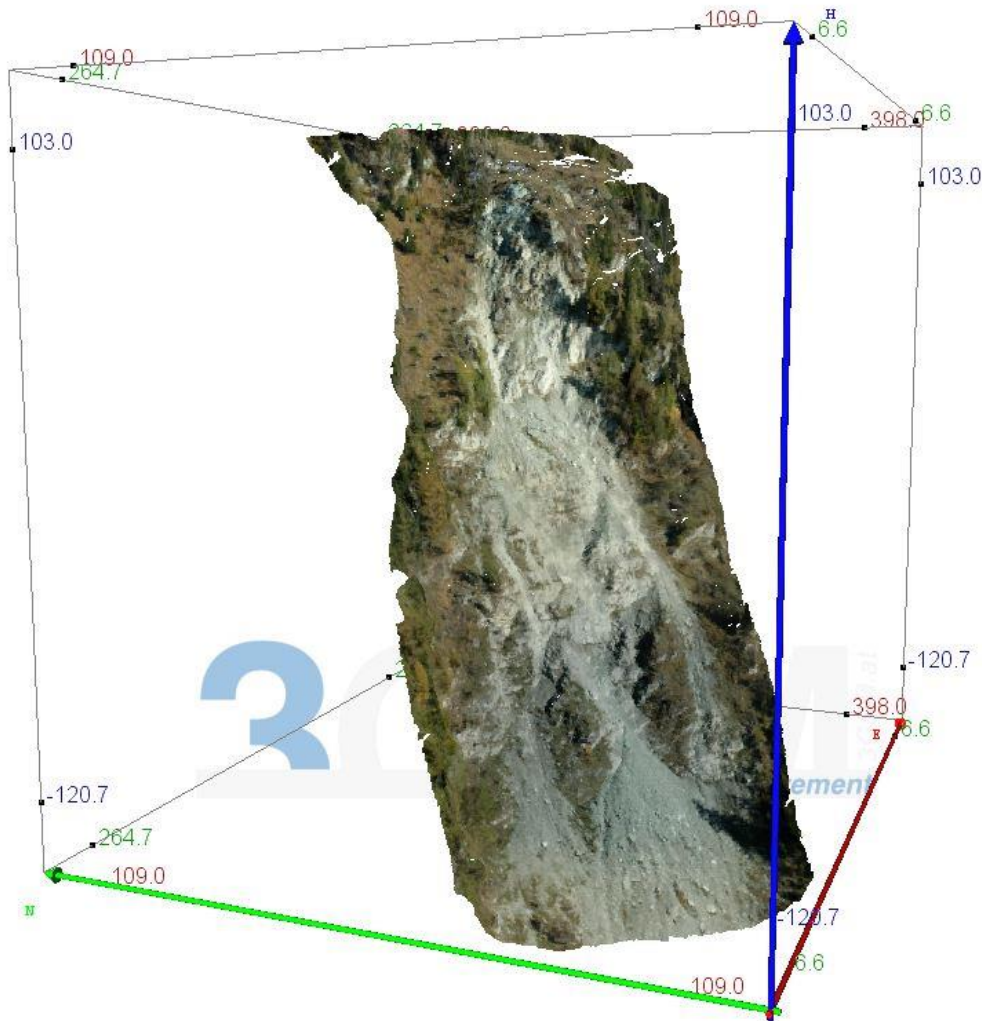


Figure 9: Scaled and referenced 3D surface model of the Ingelsberg rock slope generated with ShapeMetriX3D v4.2 (3GSM GmbH).

Another important source of information is a digital terrain model (DTM) provided by the Geodetic Department Salzburg and the Geological Survey Service of the State Salzburg (Mag. Gerald Valentin) (SAGISOnline 2019). This DTM will be used for generation of the slope surface geometry in the 3D model created in 3DEC and thus for further numerical analyses (Chapter 262.3). The DTM will also help in the detection of the weak layer positions and their thicknesses in the geological setting of the Ingelsberg slope. For this purpose, longitudinal sections cut through the slope surface will be used (section 2.3.3).

2.2 Joint network characterisation

In this thesis, SMX Analyst is used to map and characterize the joint network in the Head Area. The mapping is user-controlled and enables the joint network characterization regarding the joint orientation, joint set spacing, trace length etc. It also allows an automated clustering of

the mapped joints into distinct joint sets (3GSM GmbH 2018).

Joints are mapped either as joint traces or explicit joint planes. The determination of the geometric parameters like the set normal spacing and the trace lengths is performed by the Multiple Scanline tool. The joint network characteristics include statistical parameters about:

- Joint set orientation (dip direction, dip angle, cone of confidence, angle of aperture)
- Joint set spacing (mean set spacing, median set spacing, standard deviation)
- Joint set trace length (mean trace length, median trace length, standard deviation)

According to the findings of Wilhelmstötter (2013), the mapped structures were clustered into four distinct joint sets. The set orientations were compared to the field data acquired and evaluated in (Wilhelmstötter 2013). The comparison is described in section 3.1. The results from the 2012 model are preferably compared to regions four and five which are closest to the active rock slope area. Hands-on mapping was not possible to carry out in the Head Area due to restrictions in the accessibility. Therefore, only photogrammetry results of the 2012 investigations are available from the Head Area.

This information is then used to generate a statistical representation of the joint network in the 3DEC model. However, the automatic statistical evaluation will not be used because the 3D model is composed of many regions of the active landslide but covers also areas of no interest. The active regions are apart from each by tens of meters but the information about the spacing is for example still covered in one single joint set. This will probably result in a bias of mean values and standard deviation caused by not representative outliers in the data. Therefore, such unrealistic values will be excluded from the data sets and new statistical evaluation will be done.

2.3 Numerical analyses

The slope stability is numerically investigated with the 3D distinct element code 3DEC v.5.2 (Itasca Consulting Group Inc. 2019b). The model considers the actual slope topography as well as the mapped joint network, derived from the mapping results (chapter 3.1). It also includes a separation between weak and competent layers at the actual heights. As described in section 1.4, the toppling mechanism is expected to be the main mechanism responsible for the continuous rock falls. All steps covered in the numerical analyses are described in Table 4.

2.3.1 Model geometry

The slope geometry is based on the actual DTM. The model was cropped by approximately 5 m in each direction except for the head, to ensure smooth boundary edges. Since the aim of the numerical simulation in this thesis was primarily defining a range of material parameters and to reconstruct the toppling mechanism, the model size was further reduced, until a slope section with dimensions of 10 x 10 x 10 meters (small model, see Figure 17) and 60 m (x-dir.), 50 m (y-dir.) and 70 m (z-dir.) (medium model, see Figure 18) located approximately in the centre of the active landslide was obtained (see Figure 10).

The model is then assigned the boundary conditions. The model sides are pinned with allowed movement in two directions and disallowed in one direction. I.e. if the model boundary is parallel to the x-axis, the grid points can move along the x- and z- axis but are restricted in the y-direction. The model base is fixed in all directions, i.e. the grid points can rotate but cannot move in any direction.

The complete 3D model covers a floor plan with the dimensions of 380 x 433 m and a total area of 164,540 m². However, the area of the active landslide is about 40,000 m² only (Di Matteo et al. 2017). Hence, the 3D model is cut into several regions to separate the active area from the stable area. The stable region is modelled as a fixed boundary box.

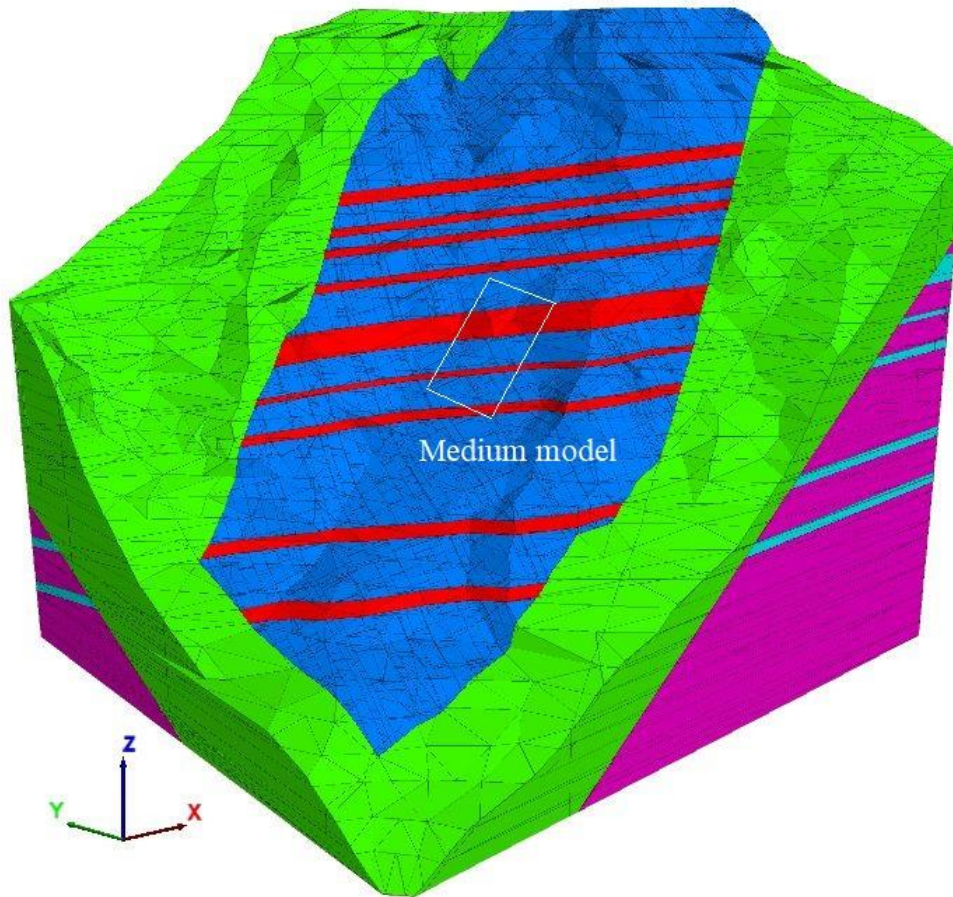


Figure 10: Approximate position of the medium model within the slope (marked by the white box). Competent rock in the active region is coloured in blue. Red coloured rock mass zones are the weak layers in the active region. The fixed/stable boundary box is coloured in green. Violet and bright blue coloured areas are the competent and weak layers in the “core” region (see section 2.3.3 – “Parallel joint”), respectively.

2.3.2 Global settings

Gravity in the model is set to be -10 m/s^2 in the z-direction. Damping is set to automatic, also called adaptive global damping. Damping controls the oscillations that may affect the final solution when tensile failure occurs. Model tolerance is controlled by command ATOL, which is set to 0.01. It is used globally to control operations in 3DEC such as minimum distance between the gridpoints, minimum area of sub-contacts, minimum block edge length etc. (Itasca Consulting Group Inc. 2019a). After all geometrical features, such as joint sets and weak layers are implemented, the model can be meshed. In this case, blocks which are smaller than 0.5 m^3 are deleted, due to their negligible influence on the global slope behaviour. Remaining blocks are meshed in two steps. Firstly, blocks with volume up to 2 m^3 are meshed with edge length

of 1 m. Secondly, all other blocks are meshed using the edge length of 2 meters, which is then maximum edge length of the mesh elements. No sensitivity analysis studying the influence of the mesh size on the model response and behaviour was performed.

Unlike in the rigid block approach used in Calvetti et al. (2018) and Vanneschi et al. (2019), the blocks in the model are deformable since the deformation of the weak layers is important for the overall toppling behaviour.

2.3.3 Geological units

A separation between rather competent green schist layers and more deformable calc-mica schist layers was done. The separation of both units follows the general orientation of the foliation. However, the foliation is not included as a distinct joint set, since it is expected that foliation joints of the material have marginal effect on the toppling mechanism studied in this thesis.

Weak layers

In order to proceed with the modelling of the Ingelsberg rock slope in 3DEC, the position and thickness of the weak layers must be known. The main indication for the position of the weak layers are changes in the inclination of the surface. It was assumed that steep inclination angles indicate competent rock masses, whereas lower inclination angles indicate weak layers. This is caused by a lower resistance against erosion of the calc-mica schists.

To locate changes in the slope inclination, certain different approaches were used and compared to confirm consistency of the results. Firstly, the online platform SAGIS (SAGISOnline 2019) was used: Several 2D cross sections (see Figure 11, possible positions of the weak layers are highlighted in red) through the landslide and the adjacent area were made and exported with the length and elevation information.

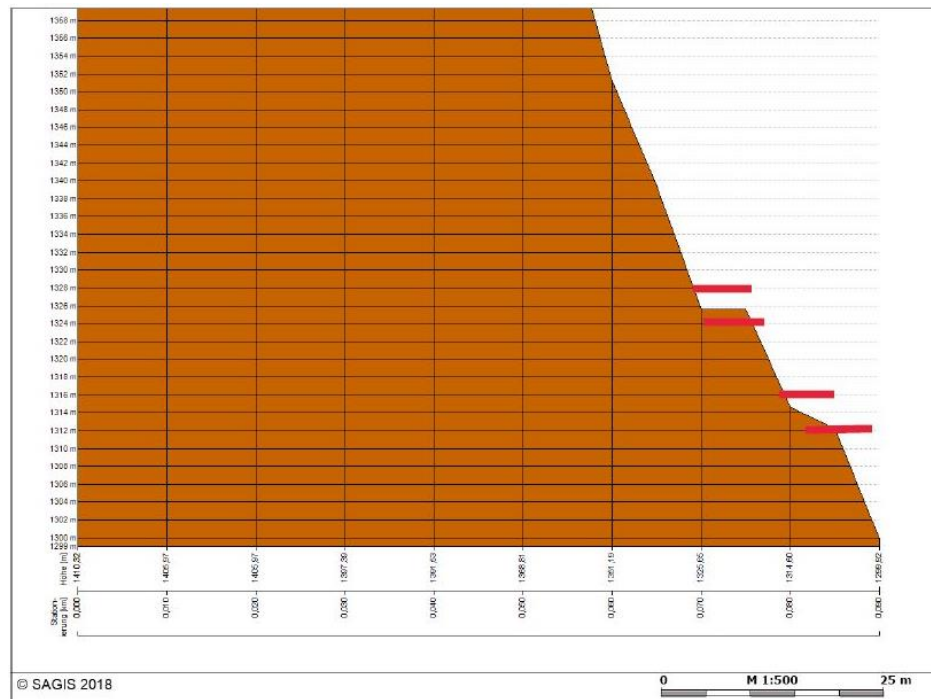


Figure 11: Exemplary 2D cross section through the slope at the Ingelsberg landslide, scale 1/500, exported from SAGIS online; the red lines indicate lithological boundaries between weak and competent layers (SAGISOnline 2019).

As a second source of information, SAGISOnline allows users to create a contour map of the surface inclination. This was done to get an overall impression about the surface because some of the features might be neglected when using the cross-sections only. This inclination map has a resolution of 1 m². Nevertheless, it is relatively hard to determine the exact boundaries of the potential weak layer. Therefore, this tool serves to support the results from the interpretation of the 2D cross-sections. Figure 12 shows the inclination map, with steep slope angles indicated in red and flatter surface patches displayed in yellow and green. Height points were used to position the irregularities in the slope inclinations.

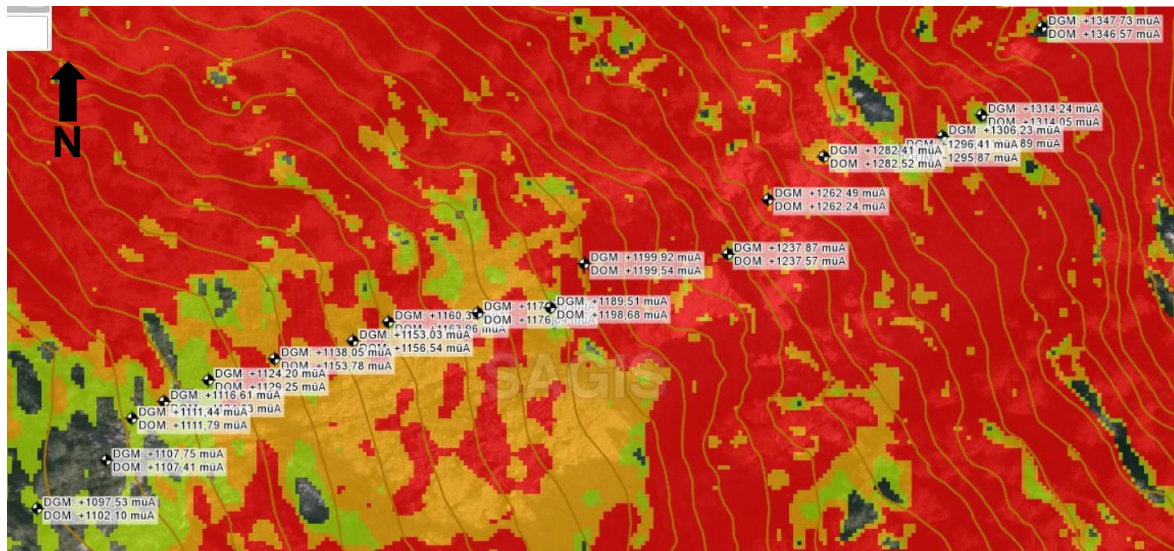


Figure 12: Plan view of the surface inclinations, exported from the SAGIS online; Red colour indicates steep regions of the slope, orange and green indicate flatter parts and no colouring (orthophoto) means almost flat surface. Query points with elevation information were used to detect the potential weak layer positions (SAGISOnline 2019).

The last approach to determine the elevation and position of the weak layers is similar to the first approach: It also compares the inclination of the surface from sections cut through the surface model. However, in this case a DTM was used to generate the 2D cross-sections. The DTM appears to be the most reliable source of information with its high resolution (grid cell size = 1 m²). The DTM is based on MGI M31 coordinate system.

In this case, three different cross-sections were analysed to get reliable results. The first cross-section is located directly at the active landslide, the second passes through the “north wall” northwest from the active landslide and the third section is located at the “backslope” southeast from the active area. Figure 13 shows the cross-section through the active landslide derived from the DTM (notice the protective dam at altitude of 1080 m highlighted by a red circle). The scale is different in height and length, namely by ratio 2:1.



Figure 13: 2D cross-section through the active landslide derived from the GIS application QGIS (DTM), the elevation is over-scaled by 2:1. The red circle highlights the position of the protective dam.

Parallel Joint

A so-called Parallel Joint is created artificially to decrease the computational effort and to unite the stress conditions for the surface of the slope which is the part of the main focus. The artificial joint is parallel to the average slope surface. The depth is approximately 20 m below the surface. Average orientation of the slope surface and the parallel joint is $246/41.8^\circ$. The rock mass (“Core Region”) underneath the joint is not jointed, whereas above, the mapped joint sets were introduced. The alignment of the two regions, separated by the Parallel Joint, is shown in Figure 16.

Also, properties of the weak layers are modelled differently: underneath the Parallel Joint, the material of the weak layer is assumed to be unweathered and has therefore a higher stiffness than in the weathered zone above the Parallel Joint (“Surface Region”). If the stiffness of the weak layer in the core region is set low as well, the whole weak layer gets squeezed out from the core region towards the surface due to higher applied stresses. The explicit material properties are given in Table 2.

2.3.4 Material parameters

The following chapter describes the material properties, which are used in the calculations. These properties are connected to the rock material, namely the calc-mica schist, which forms the weak layers and the green schist, which forms the competent layers at Ingelsberg. The geological setting also includes the black phyllite. However, the layers of the black phyllite are located beneath the analysed rock slope and are not considered in the calculations.

The material property values and their ranges were taken from literature (Hoek and Brown 1980; Lama and Vutukuri 1978) and from the database of tested rock specimen (RMT 2019) and adjusted according to engineering judgement. Missing parameters, like the bulk and shear modulus, are calculated assuming an isotropic linear-elastic material behaviour (Schweiger 2018):

$$K = \frac{E}{3(1 - 2\nu)} \quad G = \frac{E}{2(1 + \nu)}$$

The author is aware that schists have rather anisotropic behaviour, but no relevant information was found to reliably describe the anisotropy. This might be improved by future laboratory tests, which would examine the real parameters of the calc-mica schists forming the weak layers. For the values of calc-mica schists, an assumption of very weak material was done. This material must be deformable to secure the toppling mechanism of the rock towers. Another feature for the numerical model was the division of the weak layers of calc-mica schists into weathered and unweathered. This arrangement is shown in Figure 16, where the slope is divided into a “surface” and a “core” region. All parameters are summarized in Table 2 and their position in geological cross-section with parameters is shown in Figure 14.

Table 2: Intact rock material properties

Material		Green schist	Calc-mica schist "core"	Calc-mica schist weak "surface"
Density	[g/cm ³]	2.78	2.75	2.72
Poisson's ratio	[-]	0.1	0.16	0.29
Young's modulus	[GPa]	30	10	1.5
K – Bulk modulus	[GPa]	12.500	4.902	1.190
G – Shear modulus	[GPa]	13.636	4.310	0.581

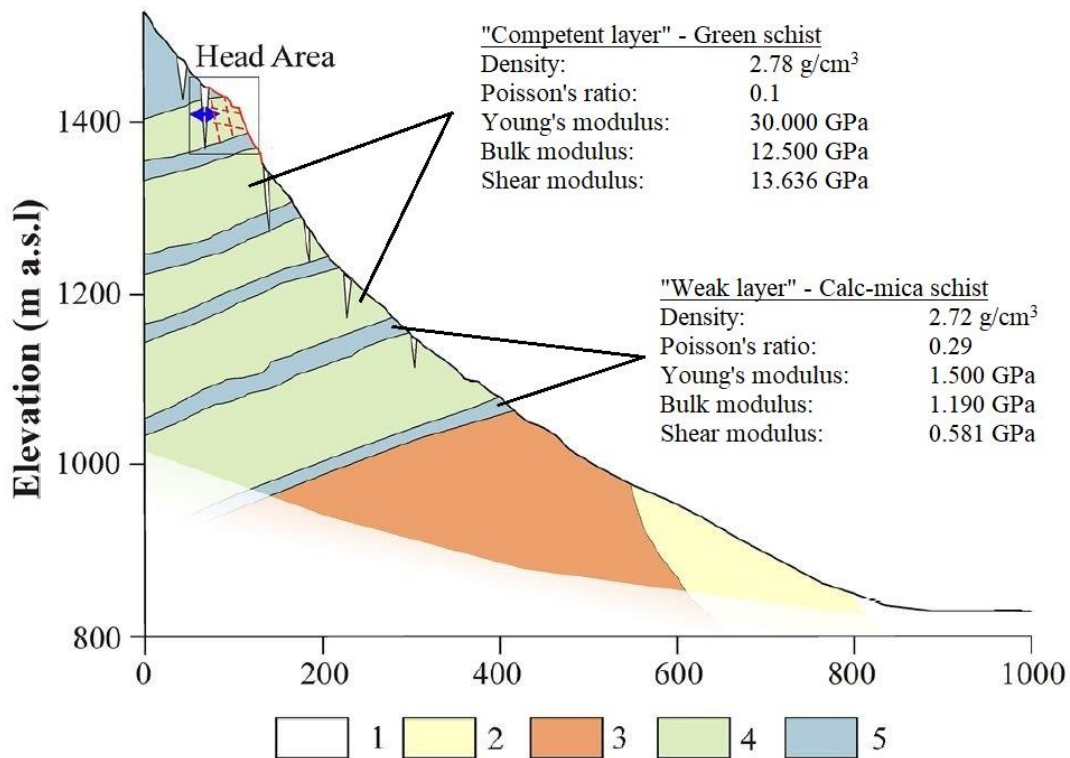


Figure 14: Arrangement of geology with properties, modified after Di Matteo et al. (2017); 1 Alluvial deposits, 2 Moraine deposits, 3 Black phyllites, 4 Green schist, 5 Calc-mica schist.

2.3.5 Joint parameters

Joint stiffness parameters are unfortunately unknown and it is practically impossible to find any reliable values in literature. Hence, the determination of realistic joint stiffness parameters is one of the main objectives of this thesis. Nevertheless, many assumptions can be done according to various guidelines. One of them deals with lower and upper boundaries for the joint normal and joint shear stiffness. These values are determined in correspondence to proper functionality of the numerical model and calculations. Mohr-Coulomb criterion was used for the joint parameters.

There are three different joint contacts in the system and thus three different parameter sets (Figure 15). The first is called "Block-block" and describes the joint parameters between the competent rock blocks which are composed of green schist. To determine the parameters, the laboratory results database of the Institute of Rock Mechanics and Tunnelling at TU Graz was used (RMT 2019). Namely, shear tests of green schists were taken for the joint parameters. The database has information from seven specimen tested. The ranges are relatively broad with friction angle differing from 23° to 41.3°, dilation angle from 2.4° to 7.7° and cohesion from 0.01 to 0.19 MPa. Final values of the properties were chosen according to values which were most close to the rock types which are present at Ingelsberg and engineering judgement. Another set of joint parameters is called "Weak layer-block" and describes the contact between

weak layer composed of the calc-mica schists and blocks in the competent layer composed of the green schists. This contact is hard to interpret with help of the laboratory results which were performed for different projects. Therefore, the friction angle and cohesion were chosen with very low values.

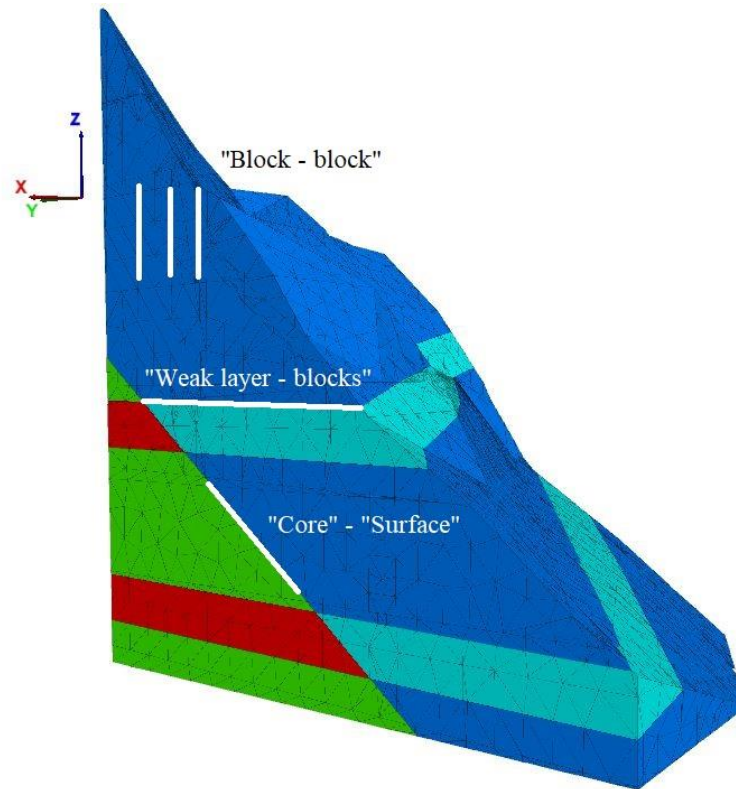


Figure 15: Model regions and joint contacts. Bright blue is a weak layer in the “surface” region, red is a weak layer in the “core” region, dark blue is a competent layer in the “surface” region and green is a competent layer in the “core” region, white bars represent the boundaries (joint contacts) between the single regions.

The third joint parameter set is called “core” - “surface” and describes the boundary between the two regions described in chapter 2.3.3. This boundary must be rigid in order to have no effect on the behaviour of the surface region. All joint parameters, chosen for the analyses, are summarized in Table 3. In the numerical analysis, sum of the friction and dilation angle is used. Tensile strength is neglected since it is presumed that all joints are already cracked. Joint normal and shear stiffnesses are not available at this stage and are subject of the consecutive research.

Table 3: Joint parameters

Contact		Block-block	Weak layer-block	"core"- "surface"
Joint normal stiffness jk_n	[Pa/m]	N/A	N/A	1.00e9
Joint shear stiffness jk_s	[Pa/m]	N/A	N/A	1.00e9
Joint cohesion	[MPa]	0.1	0.5	1000
Joint friction angle φ	[°]	32	22	89
Joint dilation angle i	[°]	6	0	0
$\varphi + i$	[°]	38	22	89

Definition of jk_n and jk_s

First value ranges of the joint normal and shear stiffness are done according to 3DEC user's manual (Itasca Consulting Group Inc. 2019a). It provides a guideline to estimate lower and upper boundaries for the values in order not to cause numerical problems. These boundaries are limited mostly by the stiffness of the rock material adjacent to the joints.

Upper bound values for jk_n and jk_s are calculated using the following formula:

$$jk_n \text{ and } jk_s \leq 10.0 \left[\max \left[\frac{K + 4/3G}{\Delta z_{min}} \right] \right]$$

Where z_{min} is the smallest dimension of zone adjoining the joint in normal direction, K is the bulk modulus and G is the shear modulus of the adjacent material.

In this case, the model is meshed with minimum edge length 1, which is also z_{min} .

For the green schist the value of the Young's modulus is set to $E = 30$ GPa and for the Poisson's ratio to $\nu = 0.1$ which leads to a bulk modulus of $K = 12.5$ GPa and to a shear modulus of $G = 13.6$ GPa:

$$jk_n \text{ and } jk_s \leq 10.0 \left[\max \left[\frac{12.5 \text{ GPa} + \frac{4}{3} \cdot 13.636 \text{ GPa}}{1} \right] \right] = 3.07 \text{ e}11 \text{ Pa/m}$$

For the calc-mica schist of the surface region of the weak layer the value of the Young's modulus is set to $E = 1.5$ GPa and for the Poisson's ratio to $\nu = 0.29$ which leads to a bulk modulus of $K = 1.19$ GPa and to a shear modulus of $G = 0.58$ GPa:

$$jk_n \text{ and } jk_s \leq 10.0 \left[\max \left[\frac{1.19 \text{GPa} + \frac{4}{3} \cdot 0.581 \text{GPa}}{1} \right] \right] = 1.96 \text{ e}10 \text{ Pa/m}$$

Since the values of stiffness and Poisson's ratio of the "core" calc-mica schist are between the values of the two other materials, it is not necessary to calculate the upper bound values.

Lower bound values are suggested to be estimated on a joint normal displacement that would result from the application of typical stresses in the system ($u = \sigma/jk_n$). Displacement should be small compared to a typical zone size. Suggested boundary for the displacement is 10 % of the adjacent zone size (1 m). There are two regions considered for the lower bound value of jk_n . The first is at the bottom of the model where stress conditions should be maximum and second determination is for the joints between the blocks and weak layer in the surface region of the model, as described in Figure 16.

First is the value for the stress level at the bottom of the model. Considering the height difference between the Head Area (altitude of 1420 m) and the bottom of the model (altitude of 1090 m), the overburden is 330 meters. Considering a gravitational loading only and with a weight density of 28 kN/m³, the theoretical maximum stress acting on the bottom joints is:

$$P = 330 \text{m} \cdot 28 \text{ kPa/m} = 9\,240 \text{ kPa}$$

$$u = P/jk_n$$

$$0.1 = 9\,240 \text{ kPa}/jk_n$$

$$jk_{n,bottom} = 92.4 \text{ MPa/m} = 9.24 \text{ e}7 \text{ Pa/m}$$

Second is the value for the stress level at the contact between blocks and weak layer in the surface region according to the Parallel joint approach. This approach is described in section 2.3.3 and in Figure 16.

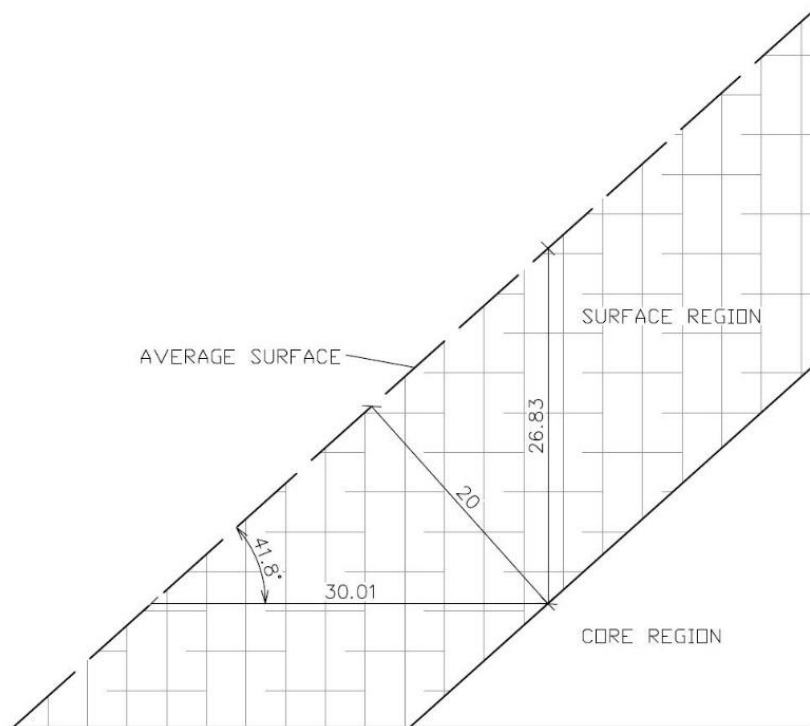


Figure 16: Surface and core regions of the model.

To calculate a new lower bound for the models with two regions, the anticipated stress levels acting on the weak layer must be calculated. Figure 16 shows that the maximum vertical distance between the surface plane and the core region is 27 meters. Thus, considering the overburden of 27 meters and weight density of 28 kN/m^3 , the stress acting on the weak layer is:

$$P = 27 \text{ m} \cdot 28 \text{ kPa/m} = 756 \text{ kPa}$$

$$0.1 = 756/jk_n$$

$$jk_{n, \text{weak layer-block}} = 7560 \text{ kPa/m} = 7.56 \text{ e6 Pa/m}$$

φ_{joint} sensitivity analysis

This chapter describes an investigation of the model response with different friction angle values for the joint contacts. The analyses were performed with a small-scale model (10 x 10 x 10 meters), which decreases the computational effort. The actual geometry of the whole slope was used, i.e. the slope was cut until the small box was obtained. The model contained one weak layer with an actual orientation 355/13 according to the foliation orientation. Additional joint sets creating the block towers which should be subjected to toppling were set simply perpendicular to each other with vertical dipping. Main objective of this small

model is to confirm the setting of hard and weak material properties. If the setting is correct, the blocks should be squeezed into the weak layer and subjected to toppling mechanism. Therefore, joint parameters were kept relatively low, $j_{kn} = j_{ks} = 1e4 \text{ Pa/m}$, cohesion 0.1 MPa . The response of the system is observed at the changing value of a maximum displacement in the model after certain number of steps. The friction angle is increased by 1° between 15° and 30° , then by 2° for each step up to 50° and by 5° steps up to 65° . The range was limited with 65° because some of the laboratory tests on schists (RMT 2019) resulted to values of the friction angle up to 40° and the dilation angle of 25° . Sum of these values (65°) appears to be rather unrealistic for the Ingelsberg slope as well as lower values in the range of 15° to 22° (lowest laboratory test value). But for this simple analysis the response of the system is of interest as well. Each calculation covers 15,000 steps after which the maximum displacement value is read. Number of steps was chosen in order to have a certain evolution of the model and to keep the computational effort low.

Figure 17 shows the smaller model from calculation with a friction angle of 23° . The thick purple layer is the weak deformable layer. For this case, toppling mechanism and opening of joints is clearly visible.

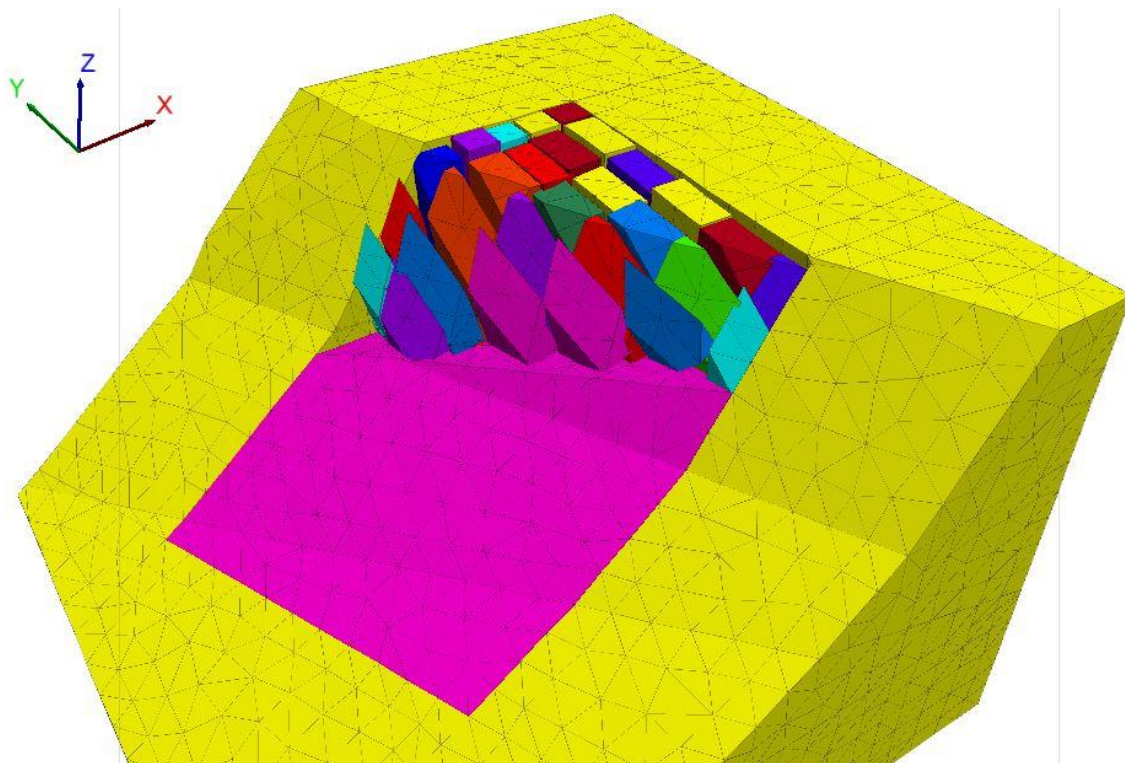


Figure 17: 3DEC model used for the friction angle analysis; the purple zone represents the weak layers, whereas the coloured blocks are the towers of the competent material formed by the intersection of K1 and K2; the yellow zone represents the rigid boundary of the model.

Sensitivity analysis jkn and jks

In order to determine more precise joint stiffness parameters, numerical analyses of the slope stability must be performed. A certain range for jkn and jks is already defined according to the 3DEC user's manual (Itasca Consulting Group Inc. 2019a). However, this range is still too large.

After the toppling mechanism in the small model is reached, a new larger model is modelled to further explore the behaviour of the slope. The model size was increased to approximately 50 x 60 x 50 m³. This model, referred to also as medium model, is an extract of the large-scale slope model and includes two interposed weak layers. At this stage, the idea of the parallel joint described in 2.3.3 is already implemented. The medium model includes only two joint sets: Joint set 1 (K1) has an orientation of 105/88 and a regular spacing of 5 meters; Joint set 2 (K2) has an orientation of 025/90 and a regular spacing of 10 meters.

In order to calculate the primary stress state (PSS), the model will be loaded with increased joint strength parameters. All joints in the system are assigned joint normal stiffness (jkn) and joint shear stiffness (jks) of 1e8 Pa/m, cohesion of 1e20 Pa and a friction angle of 89°. This high strength ensures that an equilibrium state is reached without any large movements or failure in the system (Itasca Consulting Group Inc. 2019a; Vanneschi et al. 2019). The equilibrium is reached at a maximum ratio in the unbalanced forces of 1e-6. After the PSS is reached, joint parameters are assigned according to Table 3. Since the investigated model represents a preliminary stability study, water pressure is not considered at this initial testing. Main objective of the medium model analysis is a preliminary definition of the joint stiffness parameters. The joint normal stiffness is expected to be the most controlling parameter, since a low value allows blocks to numerically overlap into each other, like the sinking of the toppling blocks into the weak layers, whilst a too high value will probably reduce or even stop the toppling mechanism. A high value of the joint shear stiffness would probably reduce the toppling as well, since the small blocks in the front should be able to slide early and enable toppling of the blocks behind. These two parameters will be studied in series of numerical simulations with different settings of parameters. Joint normal stiffness will be increased from value of 5e3 Pa/m in regular steps of 1.0, 2.5, 5.0 and 7.5 for each order up to the value of 7.5e5 Pa/m. I.e. 5e3, 7.5e3, 1e4, 2.5e4, 5e4, 7.5e4, 1e5, etc.

Movements of blocks will be logged to support the visual evaluation of the ground behaviour. Specifically, four points are chosen in the model to observe the movements during the analyses. The location of the four measuring points is shown in Figure 18 and their coordinates are:

- Point 1: X= 433255 Y= 227014 Z= 1239.97
- Point 2: X= 433259 Y= 226989 Z= 1238.26
- Point 3: X= 433237 Y= 227023 Z= 1231.68
- Point 4: X= 433250 Y= 226993 Z= 1229.99

Table 4: Single steps of numerical calculations with description

Step	Comment
1) Model generation	Generation of a slope surface and general settings such as gravity, damping and ATOL
2) Model geometry	Implementation of weak layers, joint sets and parallel joint
3) Meshing	Blocks are meshed with specific edge length
4) Boundary conditions	Model boundaries are restricted in movements
5) Material settings	Material properties are assigned
6) Calculation of PSS	PSS calculated with high joint shear strength
7) Calculation of secondary stress state (SSS)	Displacements are reset and secondary stress state is calculated with reduced joint stiffness and strength parameters. Behaviour is observed and movements are logged

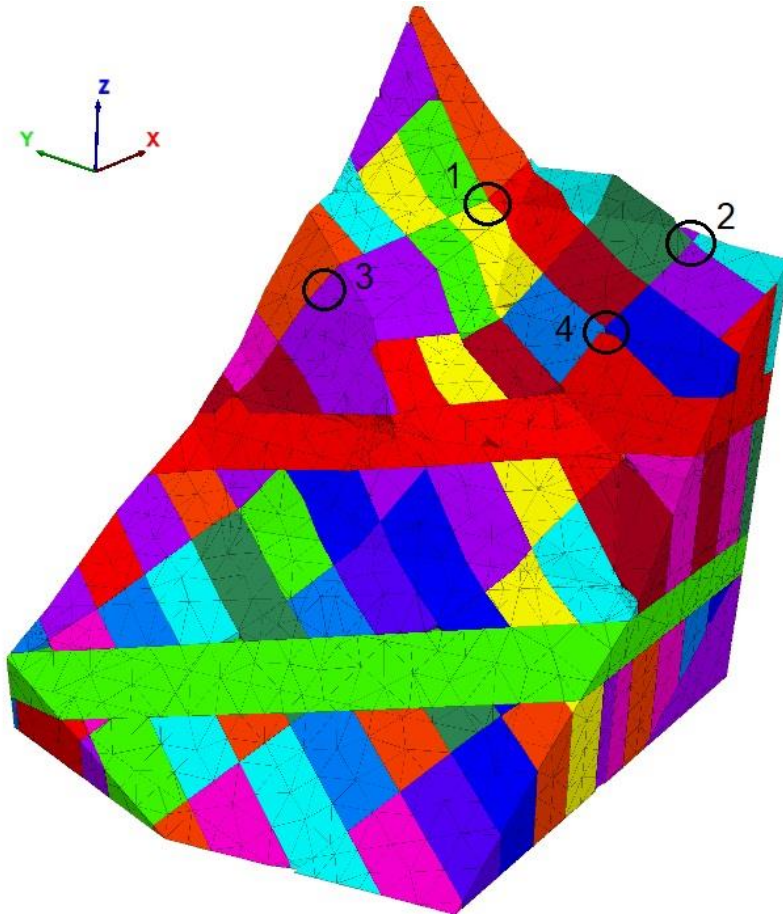


Figure 18: 4 movement measurement points for the numerical sensitivity analyses of j_{kn} and j_{ks} .

Displacements are reset after the PSS is calculated and before the loading with studied joint parameters is started.

After the joint normal and shear stiffness parameters are determined for the state where the toppling mechanism occurs and the overlap between blocks is at acceptable level, further modelling can be started. All material parameters are constant throughout the PSS and sensitivity analysis.

3 Results

3.1 Joint network characterisation

The DSM was evaluated using the SMX Analyst and the mapped discontinuities were clustered into four joint sets. The set specifications are given in Table 5 and Table 6. Figure 19 displays the pole point orientations of the mapped discontinuities (Lambert projection, lower hemisphere) along with their cone of confidence (solid line) and angle of aperture (dashed line).

Table 5: Joint set orientations of the mapped discontinuities; DD = Dip Direction, D = Dip angle, CoC = Cone of Confidence, SA = Spherical Aperture, C = Concentration.

Joint set ID	DD [°]	D [°]	CoC [°]	SA [°]	C [-]	Colour
Foliation	356	14	4.40	25.92	10.37	Lilac
K1	105	89	5.20	25.19	10.89	Blue
K2	29	79	4.09	21.58	14.61	Pink
K3	228	73	3.80	20.44	16.22	Green

Table 6: Geometrical set specifications of the mapped discontinuities in the Head Area; F = frequency, \bar{X}_s = mean set spacing, \widetilde{X}_s = median set spacing, σ_{X_s} = spacing standard deviation, \bar{T}_L = mean set trace length, \widetilde{T}_L = median set trace length, σ_{T_L} = trace length standard deviation

Joint set ID	F [1/m]	\bar{X}_s [m]	\widetilde{X}_s [m]	σ_{X_s} [m]	\bar{T}_L [m]	\widetilde{T}_L [m]	σ_{T_L} [m]	Colour
Foliation	0.08	12.56	6.20	15.04	2.47	2.16	1.53	Lilac
K1	0.13	7.52	4.52	8.76	1.93	1.39	1.79	Blue
K2	0.07	14.23	11.00	12.34	4.09	3.22	3.99	Pink
K3	0.06	16.55	13.87	11.71	3.33	1.98	3.52	Green

The geometrical and statistical information from the digital joint mapping is further on used for the definition of the joint network geometry in 3DEC. Histograms with distributions of spacing and trace lengths of the joint sets can be found in the Appendix. In order to check the reliability of the mapping results, identified set specifications are compared to field measurements given

in Wilhelmstötter (2013) with special focus on the mapping areas 4 and 5, since they are the ones closest to the Head Area.

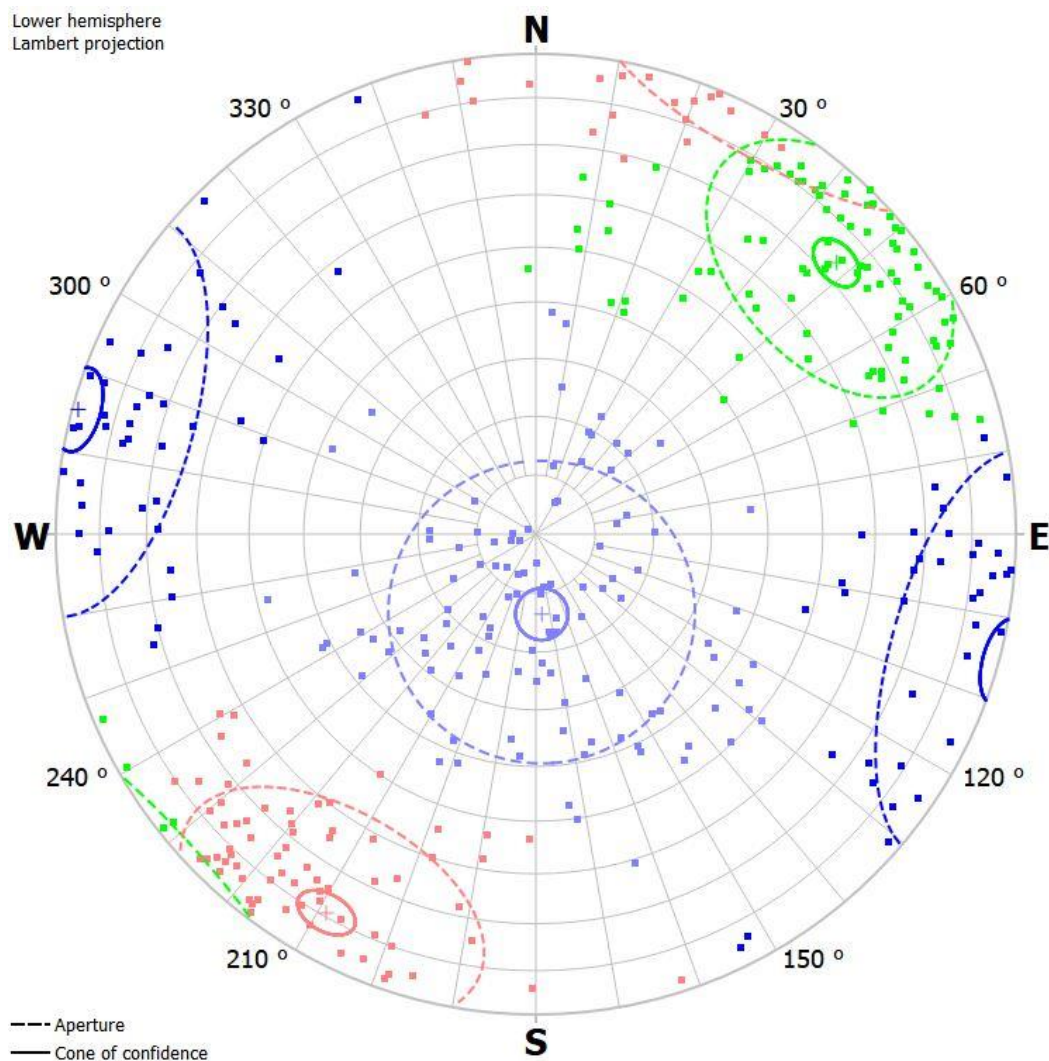


Figure 19: Lambert projection of the 2012 model joint sets, the colour of the pole points is set specific and listed in Table 5. The dashed line represents the angle of aperture, whereas the solid line indicates the cone of confidence.

Table 7 concludes information about the joint sets' geometry which were measured during a fieldwork in summer of 2012. In total, there were more than 400 discontinuities mapped in the proximity of the active Ingelsberg rock slide. Table 8 compares the values from region 5 and Table 9 compares the results with region 4.

Table 7: Absolute differences in the global orientation values of the digitally mapped joint sets (DD_{SMX}/D_{SMX}) and the joint sets according to Wilhelmstötter (2013), given as (DD_W/D_W)

Joint set ID	DD_{SMX} [°]	DD_W [°]	$ \Delta DD $ [°]	D_{SMX} [°]	D_W [°]	$ \Delta D $ [°]
Foliation	356	010	014	14	25	9
K1	105	090	015	89	85	4
K2	029	015	014	79	85	6
K3	228	230	002	73	85	12

Table 8: Absolute differences in the orientation values in region 5 of the digitally mapped joint sets (DD_{SMX}/D_{SMX}) and the joint sets according to Wilhelmstötter (2013), given as (DD_W/D_W)

Joint set ID	DD_{SMX} [°]	DD_W [°]	$ \Delta DD $ [°]	D_{SMX} [°]	D_W [°]	$ \Delta D $ [°]
Foliation	356	355	001	14	20	6
K1	105	095	010	89	85	4
K2	029	015	014	79	85	6
K3	228	235	007	73	85	12

Table 9: Absolute differences in the orientation values in region 4 of the digitally mapped joint sets (DD_{SMX}/D_{SMX}) and the joint sets according to Wilhelmstötter (2013), given as (DD_W/D_W)

Joint set ID	DD_{SMX} [°]	DD_W [°]	$ \Delta DD $ [°]	D_{SMX} [°]	D_W [°]	$ \Delta D $ [°]
Foliation	356	350	006	14	30	16
K1	105	095	010	89	85	4
K2	029	020	009	79	90	11
K3	228	N/A	N/A	73	N/A	N/A

3.2 Numerical analyses

3.2.1 Geometry – weak layers

Table 10 sums up the results of all three methods of weak layers detection. Values are sorted in ascending order. There were 9 weak layer positions detected for the active region of the Ingelsberg rock slope. These 9 weak layers were consistent through the three analysis methods. The mean thickness of the weak layers is approximately 5 m. Complete results of the three methods are summarized in Appendix in Table 14, Table 15 and Table 16.

Table 10: Positions of the weak layers

Altitudes of the weak layers considered in the active region m a.s.l.
1104 – 1110 m
1132 – 1138 m
1185 – 1189 m
1204 – 1207 m
1223 – 1238 m
1260 – 1265 m
1280 – 1285 m
1294 – 1297 m
1310 – 1318 m

3.2.2 ϕ_{joint} sensitivity analysis

Figure 20 summarizes the development of maximum displacements (not localized) with changing joint friction angle obtained during the ϕ_{joint} sensitivity analysis. It is important to note that unlike in the further calculations, the joint friction angle is same for all contacts. That means that the contacts between the blocks have the same value as the contacts between the weak layer and blocks.

This analysis showed that friction angles 32° (Block-block contact) and 22° (Weak layer-blocks contact) found in the literature are resulting in the toppling mechanism and were used for further analyses.

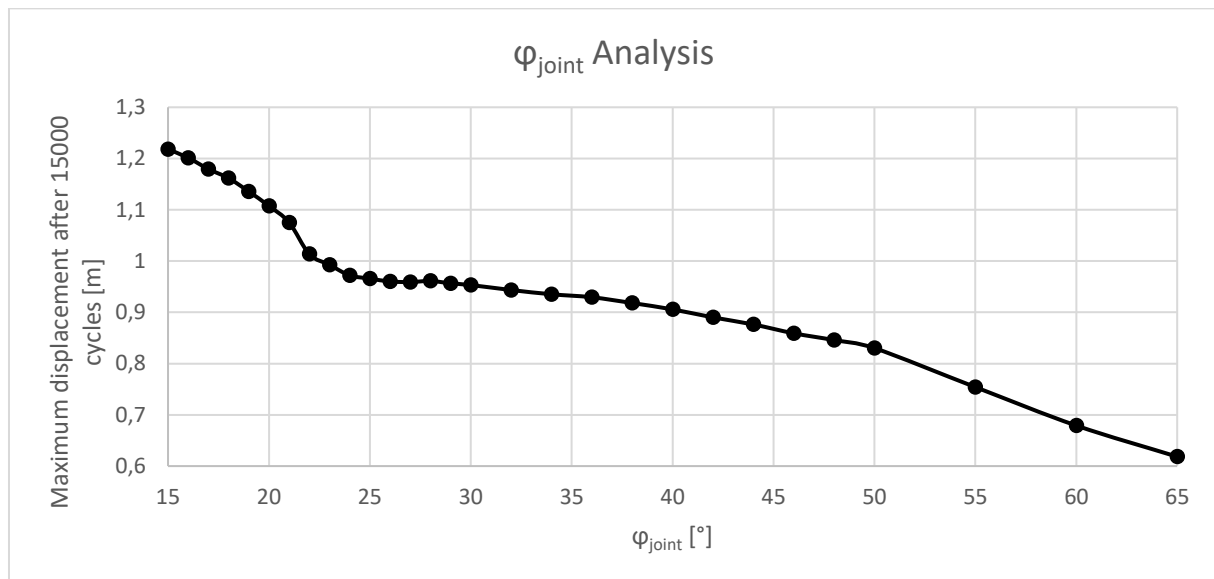


Figure 20: Block friction angle analysis showing maximum displacement in the system for a wide range of joint friction angle.

3.2.3 Sensitivity analysis jkn and jks

After the small model ($10 \times 10 \times 10 \text{ m}^3$) confirmed the appropriateness of the material parameters and to the connected toppling mechanism, the medium model was created to run a series of numerical simulations to find a range of jkn and jks values where the expected toppling mechanism is working well and overlap of the blocks is acceptable.

First series of analyses testing jkn and jks between the blocks were performed with constant value for the joint normal stiffness of $7.56 \times 10^6 \text{ Pa/m}$ for the contacts between weak layer and blocks (see section 2.3.5). This value is based on the lower bound suggestion in the 3DEC manual (Itasca Consulting Group Inc. 2019a).

Block movements were logged to support the visual evaluation and better understand the behaviour. Four points were observed through all analyses and each analysis consisted of 75,000 steps after the calculation of the primary stress state (PSS). Number of steps was chosen to restrict the calculation time needed for the analysis. Unfortunately, only displacement values in Z-direction were provided in cm precision and are used hence on. The read-out coordinates in X- and Y-direction are given only in meters. A first series of analyses was performed with a constant value of $jks = 1 \times 10^3 \text{ Pa/m}$ between the blocks. For the contact between weak layers and blocks a value of $jks = 1.5 \times 10^6 \text{ Pa/m}$ was used. Figure 21 shows movements of block point 1 with increasing value of jkn. The first 15,000 steps show an increase in the z-elevation of the observation point to a maximum of 1240.06 m. The elevation decreases afterwards until a minimum of 1239.87 m.a.s.l. ($jkn = 5 \times 10^3 \text{ Pa/m}$) is reached. No major movements are observed for jkn above $7.5 \times 10^4 \text{ Pa/m}$.

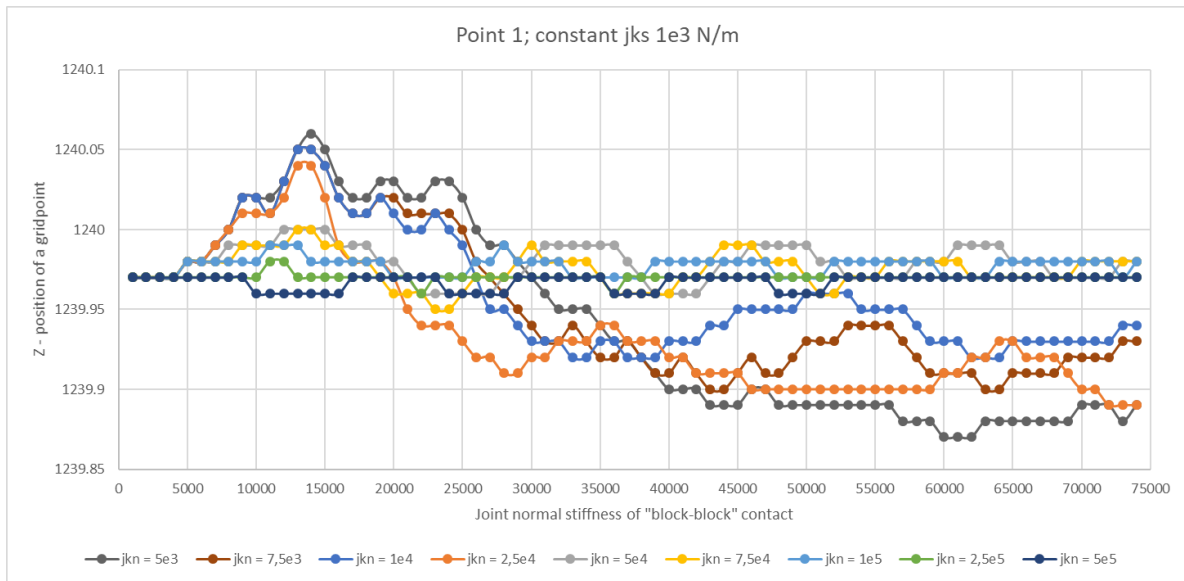


Figure 21: Point 1; movement in Z-direction with series of different jkn values and constant jks = 1e3 Pa/m between blocks.

Figure 22 shows the vertical movements of point 2.

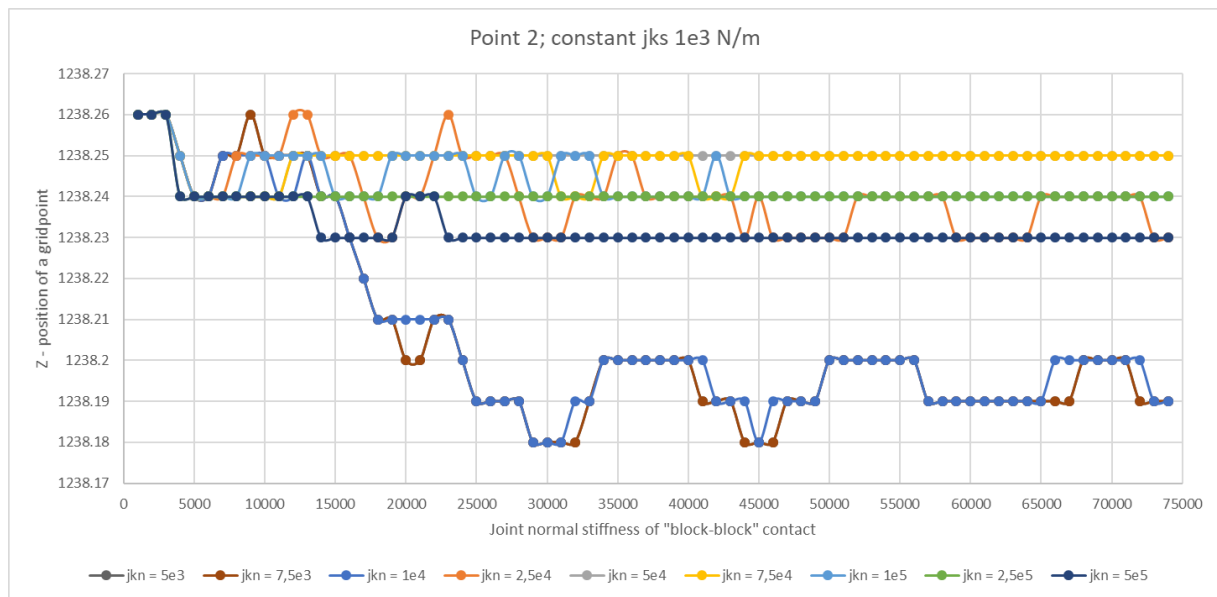


Figure 22: Movements of point 2 in Z-direction with varying jkn values and a constant jks = 1e3 Pa/m between blocks.

Since the overall behaviour with constant $jks = 1e3 \text{ Pa/m}$ between the blocks was not satisfying regarding the general response of the model and expected toppling mechanism, another series of numerical analyses was performed. The jks value in the “block-block” contact was reduced to 0 to see the response of the model and if the reduction of the jks is a right choice. The jks in the “weak layer-block” contact remains $1.5e6 \text{ Pa/m}$. Figure 23 shows movements of this series at point 3. Again, initial raising and then sinking of the observed point caused by a toppling block can be seen.

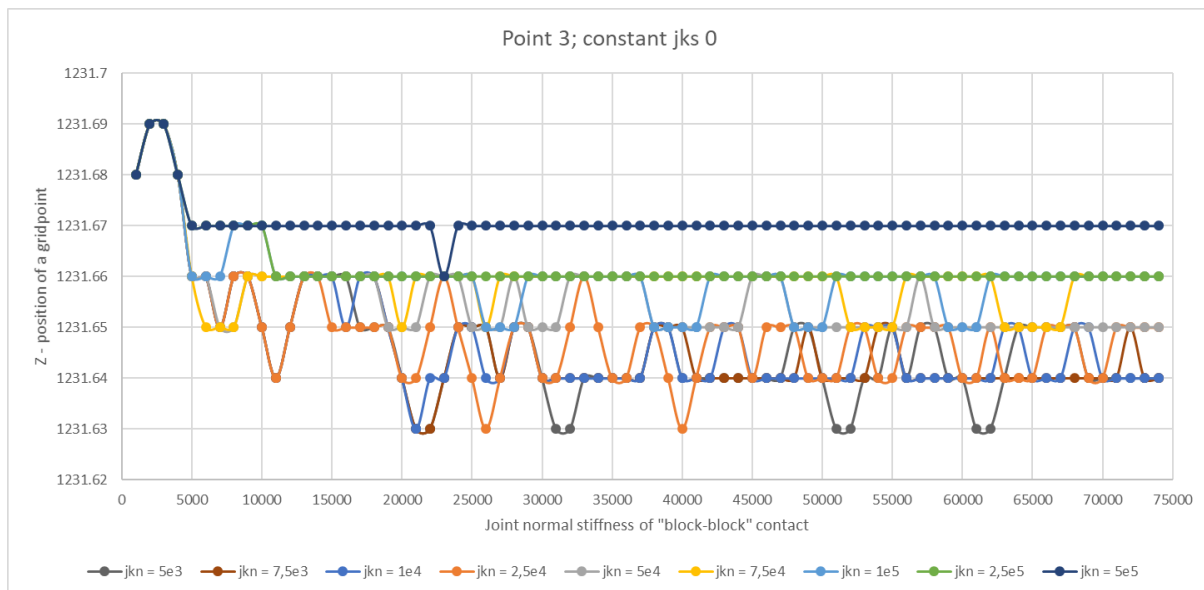


Figure 23: Movement of point 3 in Z-direction with series of different jkn values and constant $jks = 0 \text{ Pa/m}$ between blocks.

Since different values of both the jkn and jks between blocks were already tested in two series of numerical calculations without reaching a desired magnitude of the displacements of the toppling blocks, the jks between weak layers and blocks was reduced from $1.5e6 \text{ Pa/m}$ to $1e3 \text{ Pa/m}$ for another series of calculations. Joint normal stiffness differs from $5e3 \text{ Pa/m}$ up to $7.5e5 \text{ Pa/m}$.

This third series of simulations met the expectations regarding the toppling mechanism. I.e. the toppling blocks are subjected to continuous displacement development. Figure 24 shows the development of the displacements in the 3rd series with constant jks of $1e3 \text{ Pa/m}$ for both contact types. It can be seen that for jkn below $2.5e4 \text{ Pa/m}$, the model is not stable and fails after approximately 40,000 steps causing an overlap error.

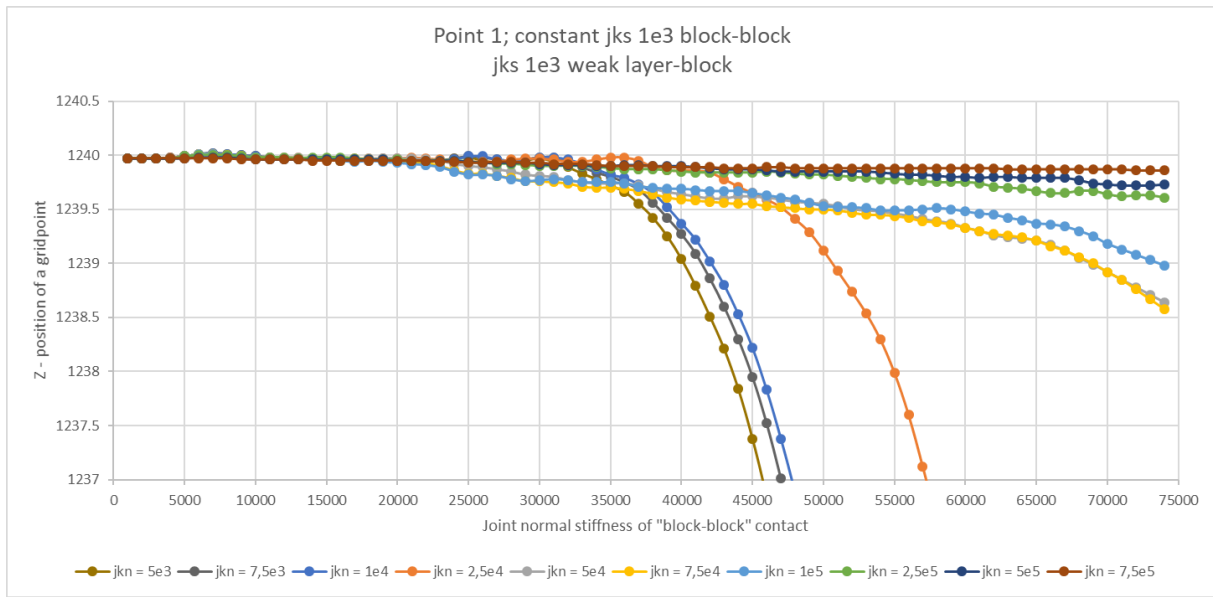


Figure 24: Movement of point 1 in Z-direction with series of different jkn values and constant jks = 1e3 Pa/m between blocks and weak layer-block contacts.

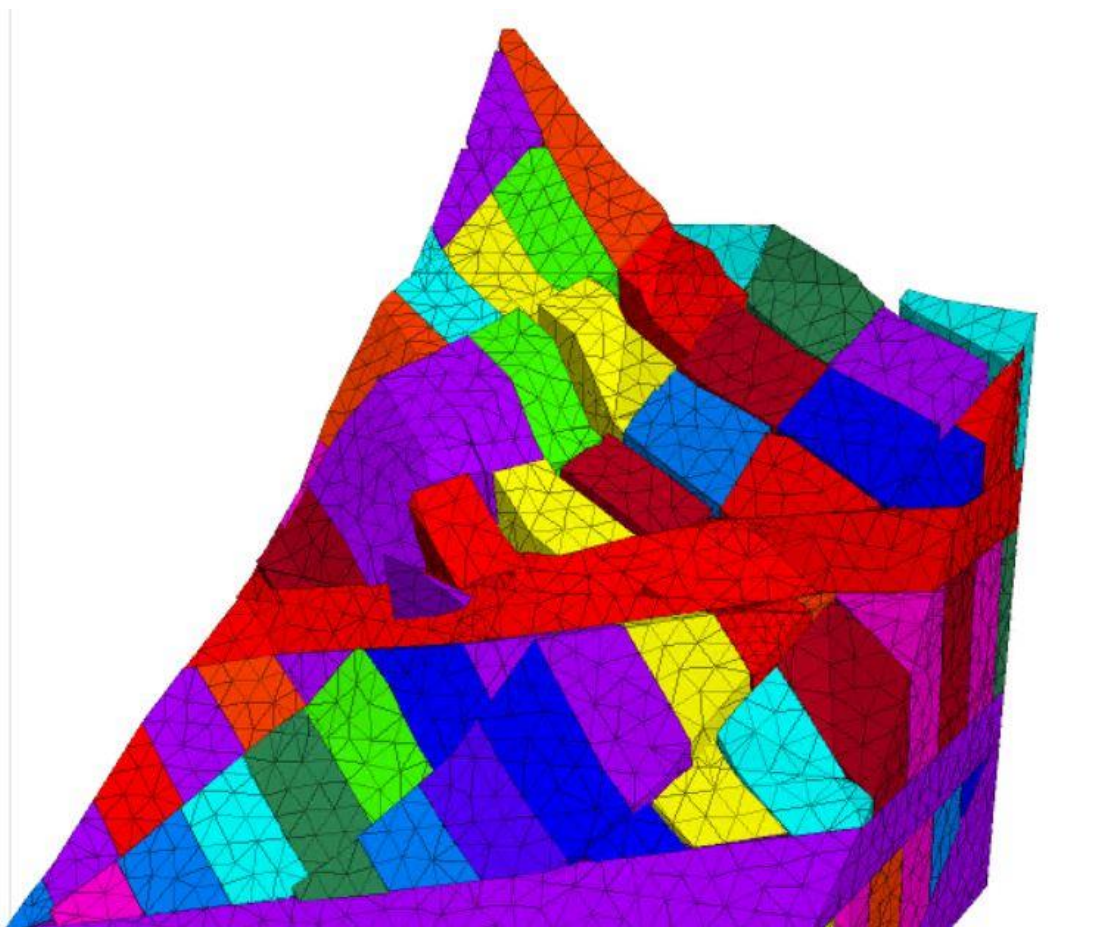


Figure 25: Toppling produced with the parameters jkn = 5e5 Pa/m ("block-block") and 7.56e6 ("weak layer-block") and jks = 1e3 Pa/m for both contact types. Capture after 75,000 steps.

In addition to previous three series, a new series of sensitivity analysis studying j_{kn} and j_{ks} inspired by Vanneschi et al. (2019) was conducted. Unlike in this thesis, the joint normal stiffness was kept constant at value of $5e9$ Pa/m for all joints. The joint shear stiffness was studied in numerical analysis. Another difference was using more calculation steps, namely 600,000. Therefore, it was decided to run a new sensitivity analysis on the medium model with the constant $j_{kn} = 1e9$ Pa/m and various values of j_{ks} for all joints. Number of steps was 600,000 as well in this series.

Joint shear stiffness was used with values $1e6$ Pa/m, $1e5$ Pa/m, $7.5e4$ Pa/m, $5e4$ Pa/m, $2.5e4$ Pa/m, $1e4$ Pa/m and $1e3$ Pa/m. For the values of $2.5e4$ Pa/m and higher, no detachments of blocks occurred and the model remained stable with small displacements. Detachments of blocks started with value of $j_{ks} = 1e4$ Pa/m. Evolution of the slope behaviour with $j_{ks} = 1e4$ Pa/m is shown in following Figure 26.

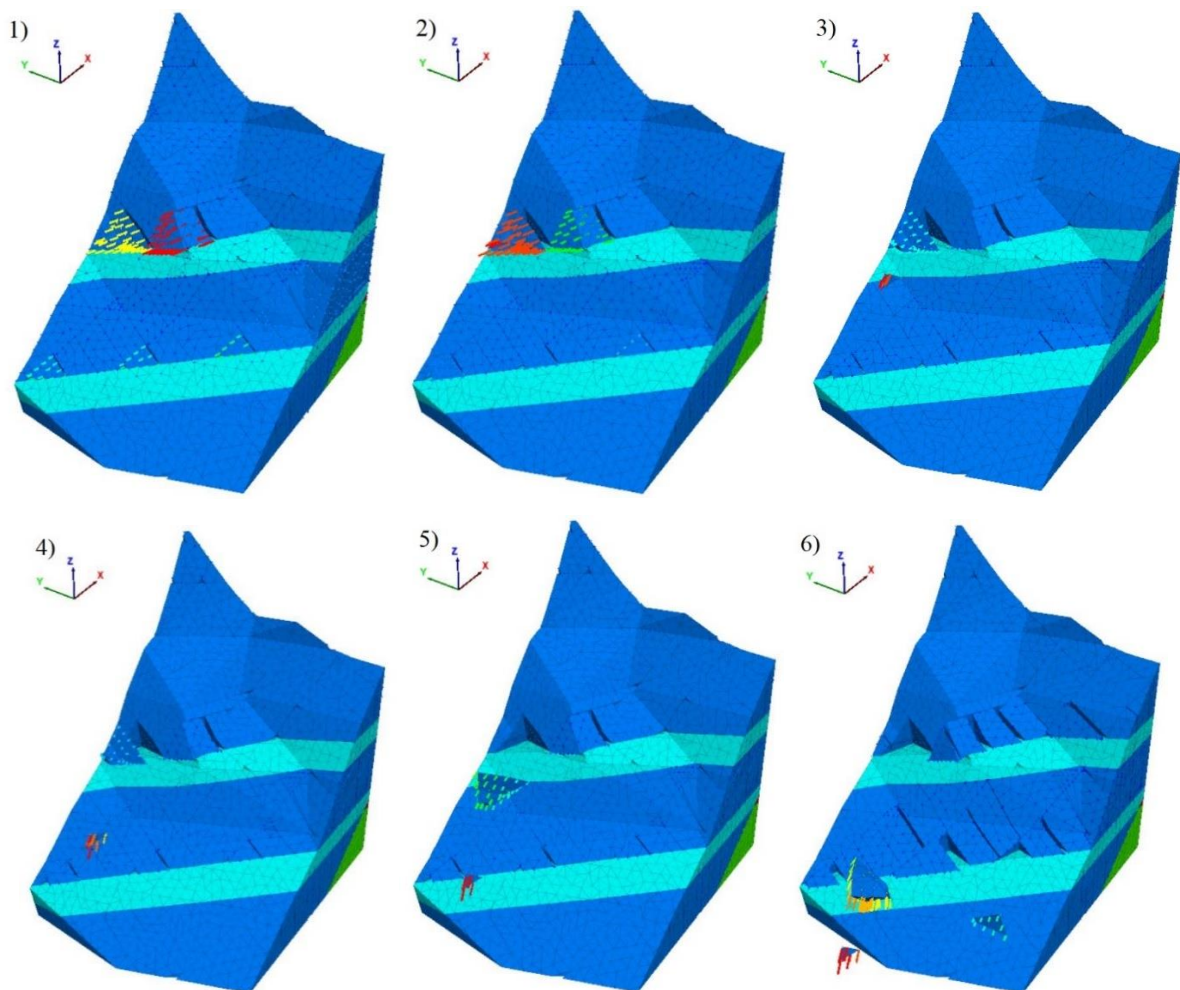


Figure 26: Evolution of the 4th sensitivity analysis series. Constant $j_{kn} = 1e9$ Pa/m, $j_{ks} = 1e4$ Pa/m. The numbers at the upper left part indicate the capture after 100,000 consecutive steps, i.e. 1) after 100,000 steps, 2) after 200,000 steps, etc. Brighter colour is the weak layer and darker the competent layer.

4 Discussion

4.1 Joint network characterization

Results of the 2012 model were compared with the findings from Wilhelmstötter (2013) in order to check their reliability and confirm usability for the numerical modelling. Table 7 shows the differences between the digital mapping results and the fieldwork (Wilhelmstötter 2013) for the overall area. This table already shows a relatively good comparability of the two data sets. A maximum deviation of 15° appears to be acceptable difference.

As already mentioned, region five proposed in Wilhelmstötter (2013) is of the most interest for the comparison, since it is located in proximity of the Head Area. Table 8 shows comparison between the 2012 model and the region five mapped by Wilhelmstötter (2013). Wilhelmstötter (2013) mapped 56 discontinuities in the region five: 21 for schistosity and 35 for the joint sets. The biggest difference in the orientations is 14° which is allowable, considering fact that not exactly the same rock masses are being compared.

Region four is another one in proximity to the active rockslide. Table 9 concludes the results of comparison between the region four and 2012 model. Wilhelmstötter (2013) concluded that only joint sets K1 and K2 are present in the region 4. There was no obvious evidence for a pattern including the joint set K3. Nevertheless, results of comparison for foliation, joint set K1 and joint set K2 show also very consistent orientations with the biggest deviation of 16.4° in the dip direction.

To conclude, results of the comparison are satisfying and it was decided that data from the 2012 model is reliable and can be used for further processing and creation of the 3D model in the 3DEC.

4.2 Numerical analyses

4.2.1 Geometry – weak layers

Unfortunately, due to the lower resolution of the sections generated in SAGIS it is not easy to clearly determine how thick these layers could be in reality. Additionally, certain height sections were not generated into the PDF. E.g. for the section through active landslide in scale 1:500 there was missing section between altitude of 1299 and 1264 m. Fortunately, by generating a PDF in scale 1:1000 this problem was solved since the missing section was generated.

Certain points detected by the second method using the surface inclinations were consistent

with the results of the previous method using the 2D cross-sections generated by SAGIS. Namely it is points at elevations 1107, 1138, 1177, 1238, 1263, 1282, 1296, 1307 and 1314. When looking at the Table 14, Table 15 and Table 16 in Appendix, it is obvious that some of the layer positions are consistent throughout the different analysis methods. Results from the third approach were taken as the reference for the other methods of analysis. The consistency of the elevation levels throughout the methods is deemed sufficient enough. Same final positions of the weak layers, which have been marked in Table 10, are also marked in Table 14 and Table 15 and show a homogeneity of the results. Therefore, results from Table 10 were taken for the future processing and modelling. Only nine weak layers from altitude of 1110 to 1318 m from Table 16 are part of the active area.

Thicknesses from the DTM analysis should be the most reliable and will be taken into account. Certain consistency can be seen also for the thicknesses of the weak layers. The thickness of all weak layers appears to be in the range between 3 and 8 m. The only outlier is the weak layer at height 1223 – 1238 m a.s.l. with thickness of 15 meters. However, based on two other methods, this weak layer could be in fact two layers which were not detected separately by the third method. The thickness of the weak layers was not estimated with the surface inclination approach, due to a lack of reliability.

4.2.2 φ_{joint} sensitivity analysis

The ground behaviour throughout the analysis shows the expected values. Certain value of total displacement even for the high friction angles is given by squeezing of the deformable weak layer which is deforming under the weight of blocks. All friction angle values resulted in toppling of the blocks. This suggests that overall stability is secured rather by joint cohesion and stiffness parameters. Decreasing the value of friction angle resulted into anticipated opening of joints. In Figure 20, the maximum displacement is almost constantly growing when decreasing the friction angle from 65° to 40°. In the range 40° to 24° the maximum displacement growth reduces and is almost at constant value between 30° and 24°. Then, after the friction angle is lower than 24°, the maximum displacement starts to grow rapidly compared to the previous development. This is very interesting, considering that laboratory test database (RMT 2019) showed range of friction angles 22° to 40° for schists. Rapid growth of maximum displacement for values lower than 24° was most likely caused by an insufficient friction between the blocks and weak layer which resulted in sliding of the blocks. This corresponds to the premise that friction angle below 20° is rather unrealistic.

4.2.3 Sensitivity analysis j_{kn} and j_{ks}

Joint stiffness parameters were studied on the medium model in different series of calculations. Few initial calculations showed that value of $j_{kn} = 4e6$ Pa/m between the blocks already reduced the toppling mechanism significantly. These calculations are not covered in the results due to randomness of the approach whose purpose was just getting a rough idea about the behaviour and response of different parameters.

Firstly, joint normal stiffness between the weak layers and block with value of $7.56e6$ Pa/m calculated as lower bound proved to be ideal in all numerical calculations. Generally, it means that the toppling mechanism was allowed whereas the overlap of the blocks into the weak layer was minimal and acceptable.

Four series of numerical analyses were performed to find the best setting of the joint normal and shear stiffness. First two series already showed some expected features in the system, e.g. higher blocks in the back were initially squeezed into the weak layer and then subjected to toppling. On the other hand, smaller blocks in the front started to slide due to forces imposed by the toppling blocks in the back. In Figure 21, point sunk after initial 15,000 steps for all j_{kn} values except $5e5$ Pa/m which is caused by progressing toppling of the block. It is visible that with increasing j_{kn} from the value of $j_{kn} = 5e4$ Pa/m the toppling mechanism is reduced and basically doesn't occur for the value of $j_{kn} = 5e5$ Pa/m. In Figure 22, the block (Point 2) is located more in the front of the model and it is clearly visible that the top point sinks and doesn't raise significantly like the point 1. This is caused by immediate sinking of the block into the weak layer and sliding instead of toppling. In the second series with $j_{ks} = 0$ Pa/m, the displacement is highly reduced for values of $j_{kn} = 5e4$ Pa/m and higher. Difference between $j_{ks} = 0$ Pa/m (2nd series) and $j_{ks} = 1e3$ Pa/m (1st series) in the "block-block" contact was not significant and did not produce satisfying improvement of the ground behaviour with regard to development of the displacements. The model showed basically the same response as with $j_{ks} = 1e3$ Pa/m, which is supported by the displacement results as well. The final displacements after 75,000 steps differ only by a magnitude of few percent.

It appears that higher joint shear stiffness between weak layer and blocks in the first two series was hindering the toppling mechanism. Third series with reduced j_{ks} in the contacts "weak layer-block" showed the desired behaviour of the ground with the progressive toppling development. Figure 24 shows that for j_{kn} below $2.5e4$ Pa/m, the system is not stable and fails after approximately 40,000 steps causing an overlap error. Nevertheless, higher values of joint normal stiffness produced numerically stable (no significant overlap) system in which the toppling mechanism worked well. This means that higher blocks in the back were subjected to toppling and pushed smaller blocks in the front which would eventually fall downhill from the slope. This behaviour is shown in Figure 25. The best behaviour was reached for the last three

values of the joint normal stiffness $2.5e5$, $5e5$ and $7.5e5$ Pa/m which already reduced opening of the joints. From the Figure 24 it appears that the model might not be stable for values of $jkn = 5e4$, $7.5e4$ and $1e5$ Pa/m with further cycling of the model.

Figure 27 shows a comparison of different jks settings with constant $jkn = 2.5e5$ Pa/m between the blocks. First two series display almost no vertical displacement of the top point caused by the reduction of the toppling mechanism to minimum. For the value of $jkn = 2.5e5$ Pa/m, the second series with $jks = 0$ Pa/m reached the same displacements in comparison to the first series with $jks = 1e3$ Pa/m.



Figure 27: Comparison of numerical series with $jkn = 2.5e5$ Pa/m.

Third series with reduced jks in the contacts between the weak layers and blocks reached the expected displacements of toppling blocks, i.e. continuous sinking. Local rising is probably again caused by rotation of the block.

Detailed description of ground behaviour with general assessment throughout the third series is summarized in the following

Table 11. Joint normal stiffness was researched in a range from $5e3$ Pa/m up to $7.5e5$ Pa/m. First steps caused that the model was not even stable with some blocks propagating through the whole model and falling. This is caused by low j_{kn} allowing the blocks to overlap into one another too significantly. Higher values of j_{kn} already showed better behaviour. Best ground behaviour was reached with the value of $j_{kn} = 5e5$ Pa/m. This value resulted into expected ground behaviour with toppling blocks which were not overlapping into one another. This model after certain development is shown in Figure 25.

Table 11: Numerical series researching j_{kn} in the “block-block” contacts; constant $j_{ks} = 1e3$ Pa/m for both contacts: “block-block” and “weak layer-block”

j_{kn} [Pa/m]	Comment on behaviour
5e3	Model not stable, blocks falling through the weak layer
7.5e3	Model not stable, blocks falling through the weak layer
1e4	Model not stable, blocks falling through the weak layer
2.5e4	Model not stable, blocks falling through the weak layer
5e4	Model not stable, blocks falling through the weak layer
7.5e4	Some blocks still propagate through the weak layer, significant overlap
1e5	Some blocks still propagate through the weak layer, significant overlap
2.5e5	Two slender blocks propagate into the weak layer. Model otherwise stable with acceptable overlap of blocks and toppling well working
5e5	Toppling works, front blocks pushed from the slope by toppling blocks in the back. No visible overlap
7.5e5	Toppling reduced but still occurs. No visible overlap

In addition to the previous three series, a series inspired by Vanneschi et al. (2019) with a constant value of $j_{kn} = 1e9$ Pa/m and various j_{ks} values was done. Vanneschi et al. (2019) concluded that the most sensitive parameter for toppling behaviour is the joint shear stiffness while the joint normal stiffness can be kept high. High sensitivity of the joint shear stiffness was confirmed also in this preliminary study. High values of j_{ks} prevented any detachments of the blocks. The failure and detachments of blocks occurred only for values of $j_{ks} = 1e4$ Pa/m and lower. However, the mechanism was not toppling but only sliding of the blocks caused by deformability of the weak layer. Toppling of the blocks was not allowed due to high rigidity of the blocks produced by using the high values of j_{kn} .

To summarize, in case of presence of the weak layer, both joint normal and shear stiffness are very sensitive for the overall behaviour of the ground. The sensitivity analysis series of the changing j_{kn} values was originally done due to difficult assumption of the stress states between the toppling blocks and to that connected calculation of the lower bound values. In the end, it was proved that low j_{kn} values result into overlapping of blocks and collapse of the whole model, which was expected. On the other hand, high values of j_{kn} change the behaviour from toppling to sliding, which was not expected. Analyses on the medium model with relatively unified stress states for the blocks on the surface showed the best behaviour in the range of $j_{kn} = 2.5e5$ to $7.5e5$ Pa/m (“block-block”). Analyses focusing more on the j_{ks} showed that this parameter is very sensitive for the ability of blocks to detach and move. High values of j_{ks} result into a stable model. Therefore, j_{ks} values lower than $1e4$ Pa/m for both contact types

are recommended for further analyses studying the toppling mechanism induced mainly by presence of the weak layer. Following Table 12 and Table 13 summarize the final material and joint parameters which are proposed by this thesis. Intact material parameters of density, Poisson's ratio and Young's modulus were not changed throughout the analyses and were kept constant. No sophisticated constitutive law was considered, only the linear-elastic behaviour of the intact rock blocks was used in all analyses. Tensile strength of the joints was not considered and therefore was set to zero. Water pressures were also not considered and dilation angle was not considered explicitly in the calculations.

Table 12: Proposed material parameters

Material		Green schist	Calc-mica schist "core"	Calc-mica schist weak "surface"
Density	[g/cm ³]	2.78	2.75	2.72
Poisson's ratio	[-]	0.1	0.16	0.29
Young's modulus	[GPa]	30	10	1.5
K – Bulk modulus	[GPa]	12.500	4.902	1.190
G – Shear modulus	[GPa]	13.636	4.310	0.581

Table 13: Proposed joint parameters

Contact		Block-block	Weak layer-block	"core"- "surface"
jkn	[Pa/m]	2.5e5 – 7.5e5	7.56e6	1.00e9
jks	[Pa/m]	1e3 – 1e4	1e3 – 1e4	1.00e9
cohesion	[MPa]	0.1	0.5	1000
Friction angle φ	[°]	32	22	89
Dilation angle i	[°]	6	0	0
$\varphi + i$	[°]	38	22	89

5 Conclusion

The preliminary study of the Ingelsberg rock slope covered initial steps for studying of the behaviour with help of the 3D distinct element method. An assumption of toppling mechanism being main feature of the Ingelsberg rock slope was taken from the previous investigations.

A 3D model for the preliminary study was modelled with implementation of the digital terrain model provided by Geological Survey Service of the State Salzburg and data from the digital surface model created by photogrammetry method in 2012 providing information about the discontinuities. Results of the digital joint mapping were compared to the discontinuity measurements provided in Wilhelmstötter (2013). The comparison showed a consistency and the mapping results were used for the numerical analysis in 3DEC. In total, four different joint sets were distinguished, including the foliation and three joint sets.

Another step was determination of the weak layer positions and their thicknesses. The methodology included three different methods which produced consistent results with an assumption of nine weak layers intersecting the active slope region. Figure 28 shows positions of the nine weak layers at elevations of 1107, 1138, 1177, 1238, 1263, 1282, 1296, 1307 and 1314m.

Literature research showed that there is a wide range of material properties for the green- and calc-mica schists which form the concerned rock mass. Properties were chosen with an assumption of higher deformability of the weak layer composed of the calc-mica schists. Values of cohesion and friction angle for the joint strength parameters were also adopted from literature research. Both material and joint parameters chosen according to literature research were confirmed suitable for the model and resulted in toppling of the rock blocks. Nevertheless, it would be beneficial to perform laboratory tests of the calc-mica schists forming the weak layer for the next studies. With more precise data about the compressibility and anisotropy of the weak material, analyses might produce more precise values for other parameters.

Numerical analyses started by creation of a small model including one weak layer and two simplified joint sets with vertical dip. Firstly, this model confirmed that proposed material parameters are suitable and result in the toppling mechanism. Secondly, sensitivity analysis studying the joint friction angle was performed on the small model. This sensitivity analysis showed that the joint friction angle is not a sensitive parameter for the toppling mechanism. Friction angle varying from 15° up to 65° always resulted into toppling of block. The only difference was the magnitude of the displacements.

Then, numerical analyses continued with sensitivity analysis of the joint normal and shear stiffness performed on the medium size model located in the middle of the active slope (actual slope surface was used) covering two weak layers. At this stage, a so-called parallel joint was

used to unite the stress levels between toppling blocks and weak layers in the studied area. This medium model included a statistical representation of the joint sets K1 and K2. The sensitivity analysis showed that both j_{kn} and j_{ks} are very sensitive parameters for the toppling mechanism controlled by the deformable weak layer. Low values of the joint normal stiffness produce an unstable model whereas high values change the toppling mechanism into the sliding mechanism. The joint shear stiffness controls the ability of the blocks to detach from each other. High values of j_{ks} resulted in a stable model without any larger displacements of the blocks (within the used number of computation steps). Value ranges for the contacts between the blocks proposed by this preliminary sensitivity analyses are:

- Joint normal stiffness: $j_{kn} = 2.5e5$ to $7.5e5$ Pa/m
- Joint shear stiffness: $j_{ks} = 1e3$ to $1e4$ Pa/m
- Cohesion: $c = 0.1$ MPa
- Friction angle: $\varphi = 32^\circ$
- Dilation angle: $i = 6^\circ$

6 Outlook

Next step of the numerical analysis is complete meshing of the full-size model. High number of blocks together with different sizes of the blocks produces large computational effort. Geometry of the model was created with implementation of all features introduced in the medium model: weak layers, joints sets and parallel joint. 3DEC did not finish meshing of the model in the time span of this thesis and it is hard to estimate time needed for the meshing. Geometry of the full-size model is shown in the following Figure 28.

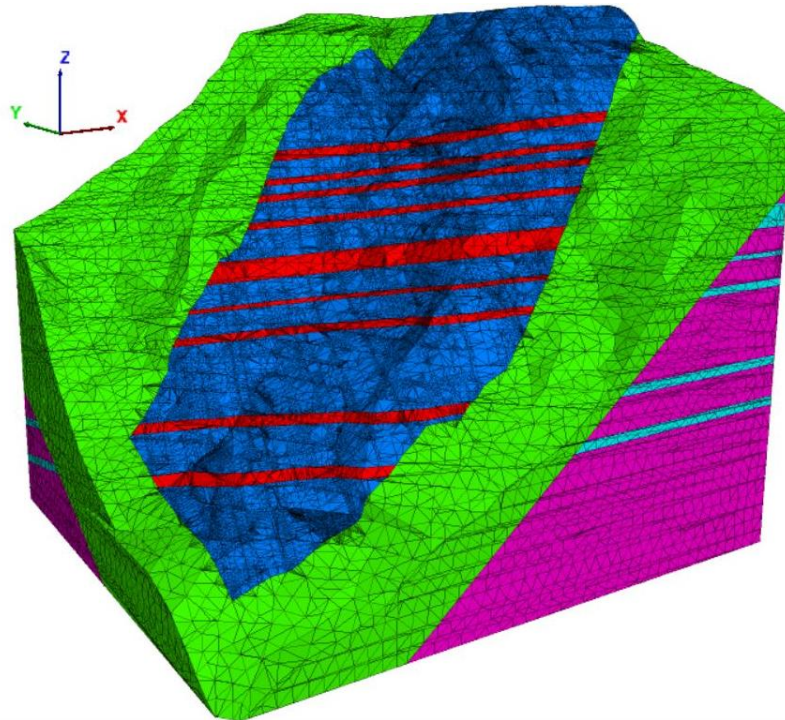


Figure 28: Geometry of the full-size model in 3DEC.

Outlook for the next analyses is completion of the working full-size model in 3DEC, followed by implementation of water/ice pressures. In order to bring the numerical analysis closer to the reality, discrete fracture network (DFN) obtained by updated scanning of the Ingelsberg surface should be implemented. This analysis would be hopefully able to detect blocks which are close to failure at the actual slope.

Missing points:

- Laboratory tests on material
- Numerical modelling of water pressure
- Installation of a precipitation gauge at the slope

7 References

- 3GSM GmbH (2018) User's manual - JMX Analyst
- Bonilla-Sierra V, Scholtès L, Donzé FV, Elmoultie MK (2015) Rock slope stability analysis using photogrammetric data and DFN–DEM modelling. *Acta Geotech.* 10:497–511. doi: 10.1007/s11440-015-0374-z
- Calvetti F, Frenez T, Vecchiotti M, Piffer G, Mair V, Mosna D (2018) DEM Simulation of the Evolution of an Unstable Rock Face: A Modelling Procedure for Back Analysis of Rockslides. *Rock Mech Rock Eng* 52:149–161. doi: 10.1007/s00603-018-1576-0
- Di Matteo L, Romeo S, Kieffer DS (2017) Rock fall analysis in an Alpine area by using a reliable integrated monitoring system: results from the Ingelsberg slope (Salzburg Land, Austria). *Bull Eng Geol Environ* 76:413–420. doi: 10.1007/s10064-016-0980-5
- Gaich A, Pötsch M, Schubert W (2017) Digital rock mass characterization 2017 - Where are we now? What comes next? *Geomechanik und Tunnelbau* 10:561–566. doi: 10.1002/geot.201700036
- Hoek E, Brown ET (1980) *Underground excavations in rock*. The Institution of Mining and Metallurgy, London
- Itasca Consulting Group Inc. (2019a) 3DEC User's manual
- Itasca Consulting Group Inc. (2019b) 3DEC version 5.2, Distinct-element modeling of jointed and blocky material in 3D. <https://www.itascacg.com/software/3dec>. Accessed 5 April 2019
- Itasca Consulting Group Inc. (2019c) FLAC version 8.1, Explicit Continuum Modeling of Non-linear Material Behaviour in 2D. <https://www.itascacg.com/software/flac>. Accessed 15 May 2019
- Jennings JE (1970) A mathematical theory for the calculation of the stability of open cast mines. *Symposium on the Theoretical background to the Planning of Open Pit Mines*. Johannesburg:87–102
- Jing L (2003) A review of techniques, advances and outstanding issues in numerical modelling for rock mechanics and rock engineering. *International Journal of Rock Mechanics and Mining Sciences* 40:283–353. doi: 10.1016/S1365-1609(03)00013-3
- Lama RD, Vutukuri VS (1978) *Handbook on mechanical properties of rocks: Testing techniques and results vol 2*. Series on rock and soil mechanics, vol 3 1978 no 1. Trans tech publications, S.I.
- Lambert C, Thoeni K, Giacomini A, Casagrande D, Sloan S (2012) Rockfall Hazard Analysis From Discrete Fracture Network Modelling with Finite Persistence Discontinuities. *Rock Mech Rock Eng* 9:1095. doi: 10.1007/s00603-012-0250-1

- Pariseau WG (2012) Design analysis in rock mechanics, 2nd ed. CRC Press/Balkema, Boca Raton
- Pestal G, Hejl E, Braunstingl R, Schuster R (2009) Erläuterungen Geologische Karte von Salzburg 1:200 000. Geologie der österreichischen Bundesländer. Geologische Bundesanstalt, Wien
- Pichler P (2013) Base Friction Laborversuche. Modellierung und qualitative untersuchungen zu Massenbewegungen im Gasteinertal. Masterproject, TU Graz
- Plaxis BV (2019) PLAXIS 2D 2019 - Material Models Manual.
<https://www.plaxis.com/support/manuals/plaxis-2d-manuals/>. Accessed 15 May 2019
- Romeo S, Scott Kieffer D, Di Matteo L (2014) The Ingelsberg landslide (Bad Hofgastein, Austria): description and first results of monitoring system (GBInSAR technique). *ROL* 32:24–27. doi: 10.3301/rol.2014.144
- SAGISOnline (2019) SAGISOnline - Salzburger Geographisches Informationssystem.
<https://www.salzburg.gv.at/sagisonline/>. Accessed 18 February 2019
- Schmid SM, Fgenschuh B, Kissling E, Schuster R (2004) Tectonic map and overall architecture of the Alpine orogen. *Eclogae geol. Helv.* 97:1–117. doi: 10.1007/s00015-004-1113-x
- Schweiger H (2018) Computational Geotechnics: part 3 Elasticity. Lecture Computational Geotechnics
- Sturzenegger M, Stead D (2009) Close-range terrestrial digital photogrammetry and terrestrial laser scanning for discontinuity characterization on rock cuts. *Engineering Geology* 106:163–182. doi: 10.1016/j.enggeo.2009.03.004
- Unterberger K (2013) The application of Ground-Based InSAR to understand slope behavior at the Hornbergl in Reutte, Tyrol and the Ingelsberg in Bad Hofgastein, Salzburg, Austria. Master's thesis, TU Graz
- Vanneschi C, Eyre M, Venn A, Coggan JS (2019) Investigation and modeling of direct toppling using a three-dimensional distinct element approach with incorporation of point cloud geometry. *Landslides* 71. doi: 10.1007/s10346-019-01192-w
- Wieser P, Kluckner A, Pilgerstorfer T, Söllner P (2012) Discontinuity mapping and photogrammetric survey of Ingelsberg landslide. Unpublished
- Wilhelmstötter F (2013) Geotechnisch-Geologische Untersuchungen des Felssturzgebietes Ingelsberg/Bad Hofgastein. Master's thesis, TU Graz
- Zekkos D, Lynch JP, Greenwood W, Manousakis J, Zekkos AA, Clark MK, Cook K, Saroglou H (2018) Lessons Learned from The Application of UAV-Enabled Structure-From-Motion Photogrammetry in Geotechnical Engineering:22. doi: 10.4417/IJGCH-04-04-03

8 Appendix

Table 14: SAGIS online – elevation of detected weak zones according to sections Active Landslide (1:500 and 1:1000) and Back Slope (1:500, 1:1000); the grey rows highlight the elevations captured in each cross-section.

Active landslide 1:500	Active landslide 1:1000	Backslope 1:500	Backslope 1:1000
	1081 – 1083		
	1099 – 1101		
1110 – 1112	1107 – 1109	1108 – 1110	1103 – 1108
		1117 – 1119	
1122 – 1124	1120 – 1123	1123 – 1125	1119 – 1123
1131 – 1134		1134 – 1136	1132 – 1134
1141 – 1143	1139 – 1141		
1149 – 1152	1146 – 1146		1151 – 1152
1160 – 1162	1158 – 1160	1160 – 1162	1160 – 1162
1178 – 1181	1176 – 1178		1175 – 1176
			1181 – 1183
	1194 – 1196	1192 – 1194	1192 – 1194
		1204 – 1206	1204 – 1206
	1211 – 1213	1212 – 1214	1211 – 1213
1226 – 1230	1226 – 1228	1228 – 1232	1225 – 1227
1239 – 1242	1239 – 1241		
	1252 – 1256	1249 – 1252	1258 – 1262
	1270 – 1272		1267 – 1268
			1275 – 1278
	1279 – 1280		1283 – 1286
	1291 – 1294	1294 – 1296	1294 – 1296
	1298 - 1300	1306 – 1308	1305 – 1307
1312 – 1315			
1324 – 1328		1322 – 1325	
		1350 – 1353	

Table 15: SAGIS online – elevation of the weak zones according to changes in the surface inclination; the grey rows highlight the elevations captured in each cross-section.

Possible weak zones according to surface inclination (MASL)	
Active landslide area	Backslope
1097	
1107	
1111	
1116	
1124	
1138	1137
1153	
1160	1158
1177	1170
1189	1181
1200	1208
1238	1241
1263	
1282	1289
1296	
1307	
1314	1312
1347	
	1365
	1372

Table 16: Weak zones according to DTM in three different cross-sections; the grey rows highlight the elevations captured in each cross-section.

Active landslide	North wall	Backslope
	1083 – 1088	
1104 – 1110		1102 – 1106
		1121 – 1125
1132 – 1138		
		1162 – 1168
1185 – 1189		1180 – 1183
		1192 – 1196
1204 – 1207		
1223 – 1238	1215 – 1218	1215 – 1222
	1240 - 1245	
1260 – 1265		1251 – 1257
	1270 – 1277	
1280 – 1285	1285 – 1287	1282 – 1286
1294 – 1297		1293 – 1295
1310 – 1318	1300 – 1315	1309 – 1312
		1329 – 1331
		1340 – 1343
	1358 – 1363	1355 – 1358
1361 – 1366		1367 – 1369
1383 – 1385		
1392 – 1395		

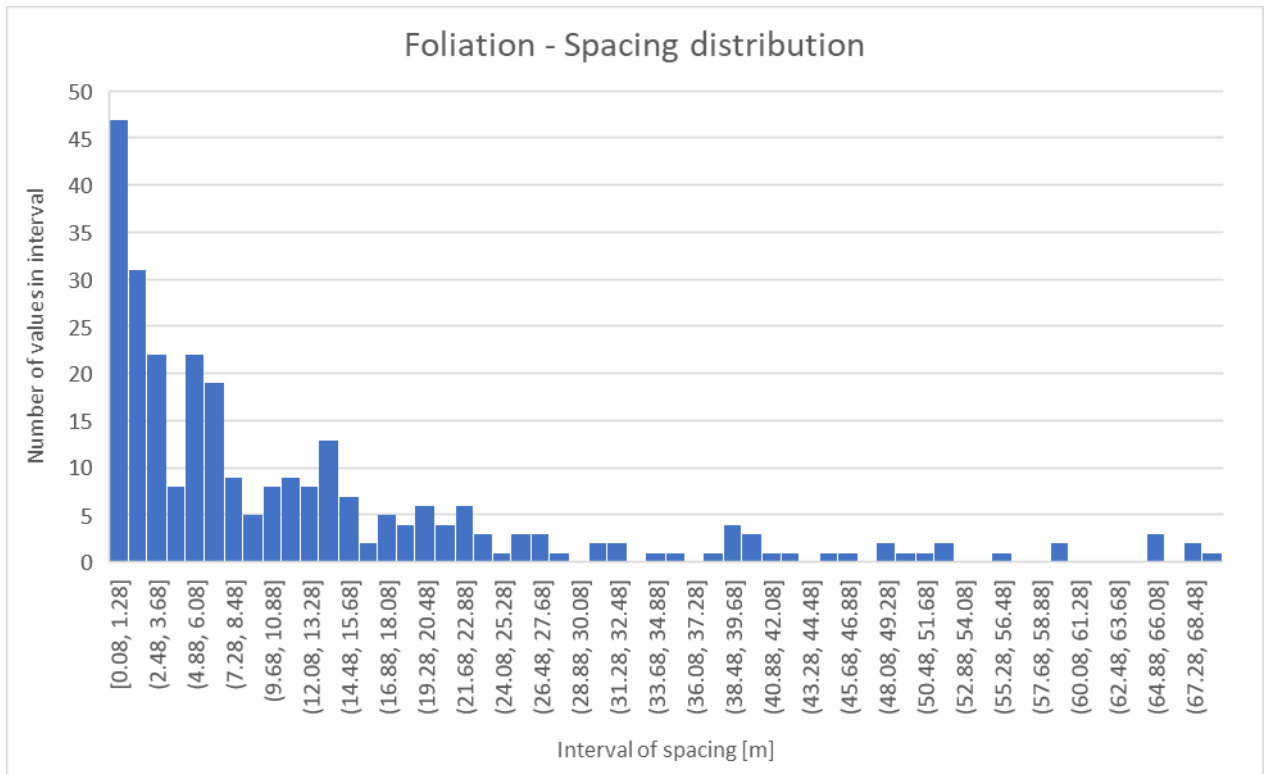


Figure 29: Foliation - spacing distribution histogram

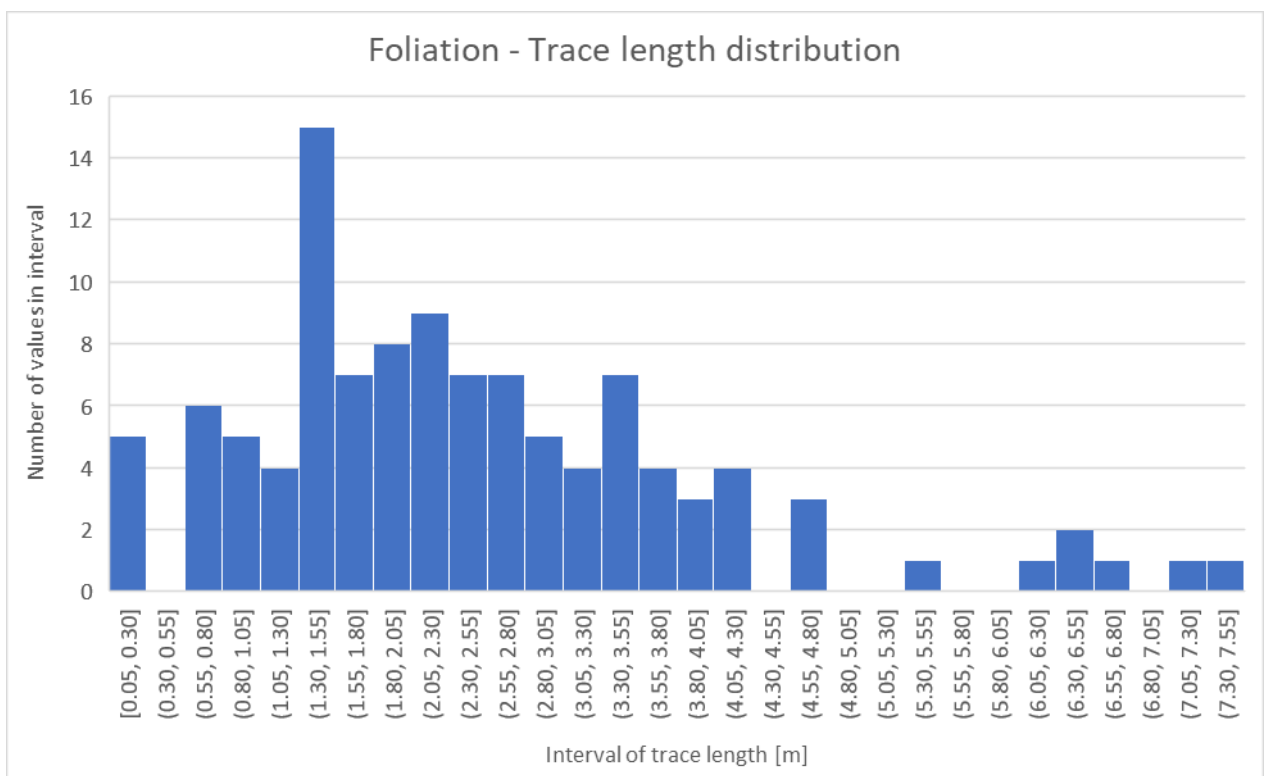


Figure 30: Foliation - trace length distribution histogram

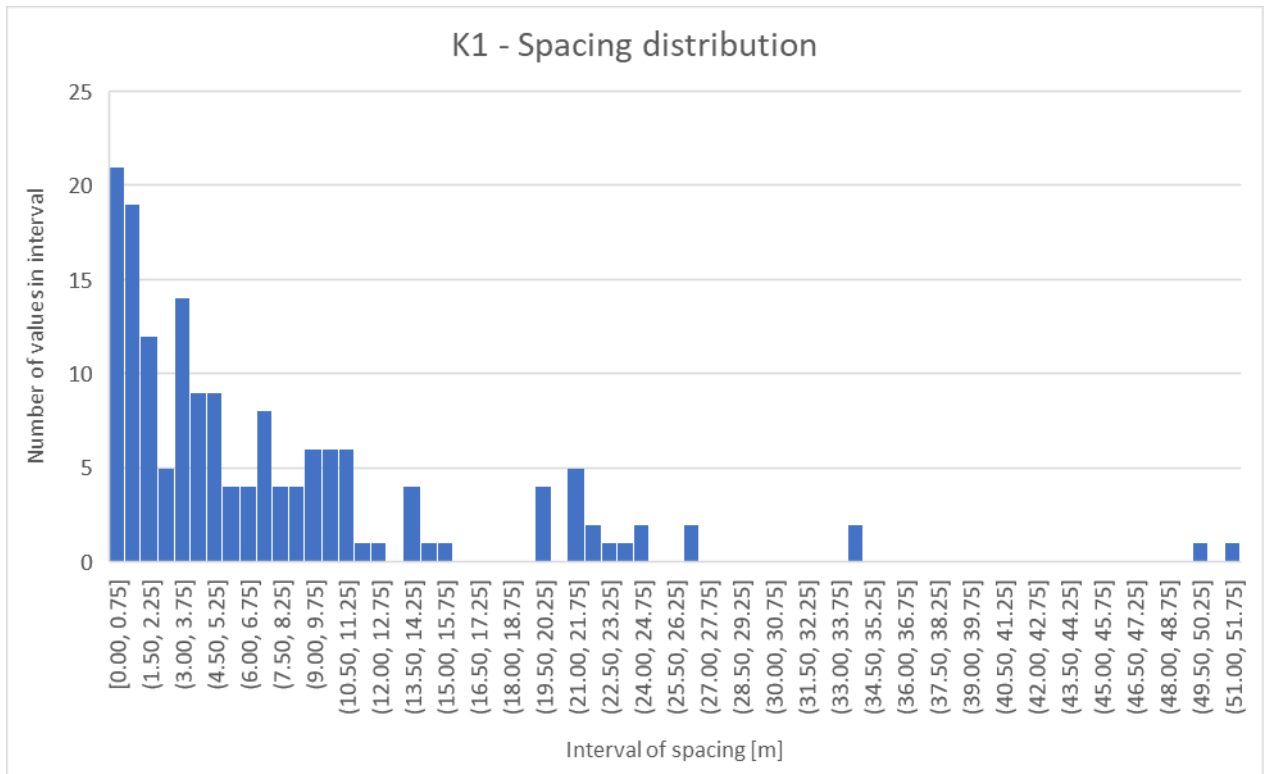


Figure 31: K1 - spacing distribution histogram

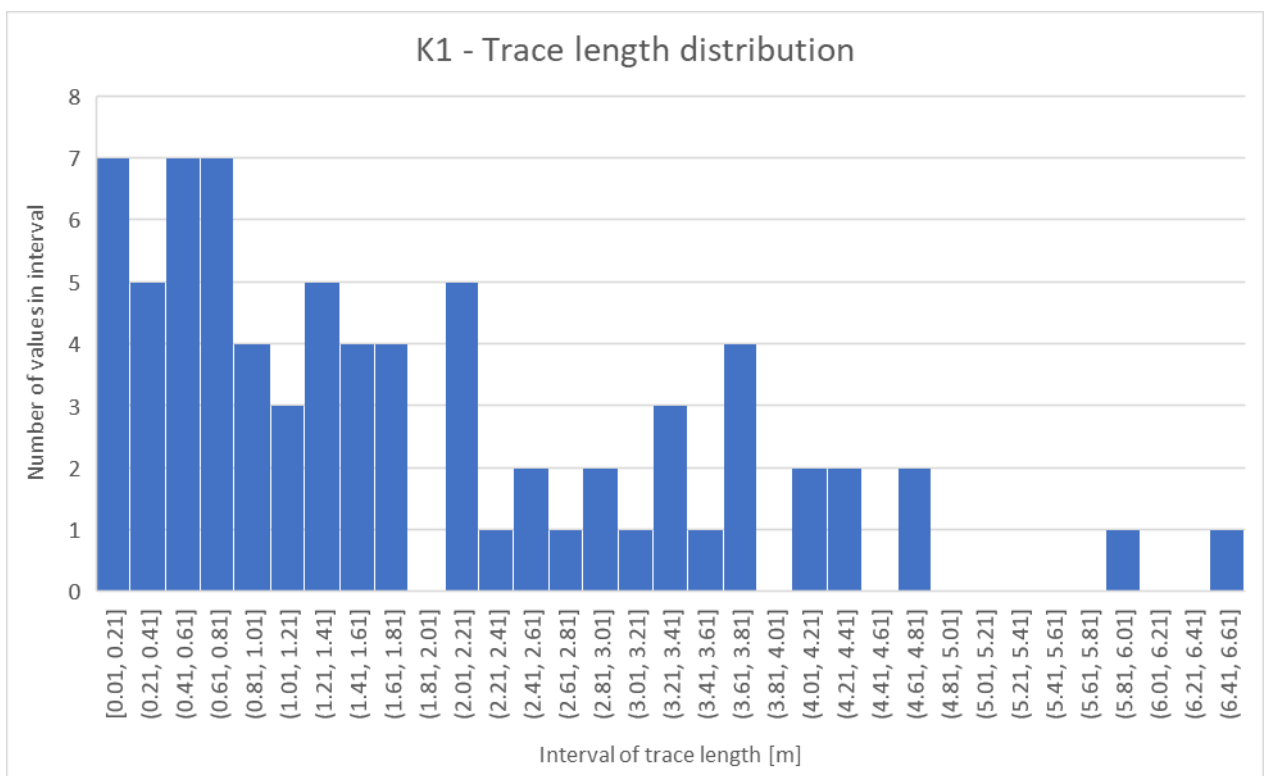


Figure 32: K1 - trace length distribution histogram

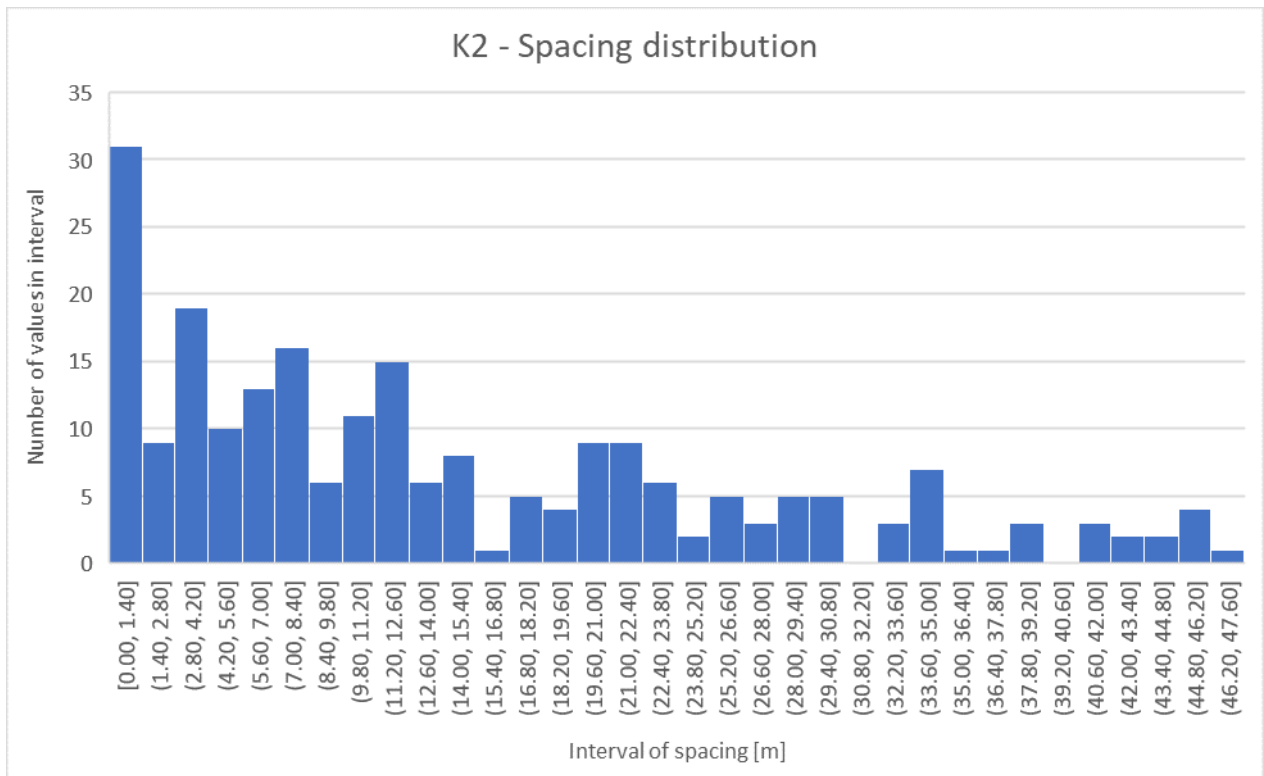


Figure 33: K2 - spacing distribution histogram

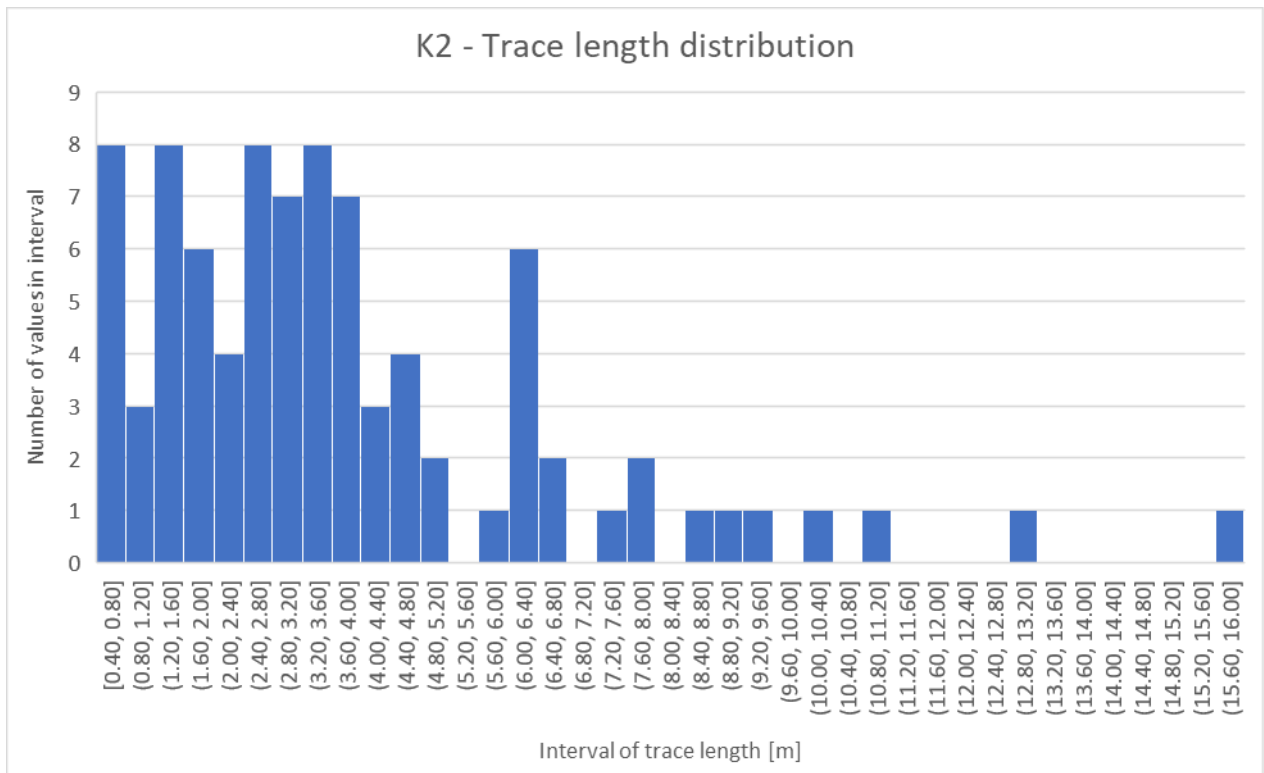


Figure 34: K2 - trace length distribution histogram

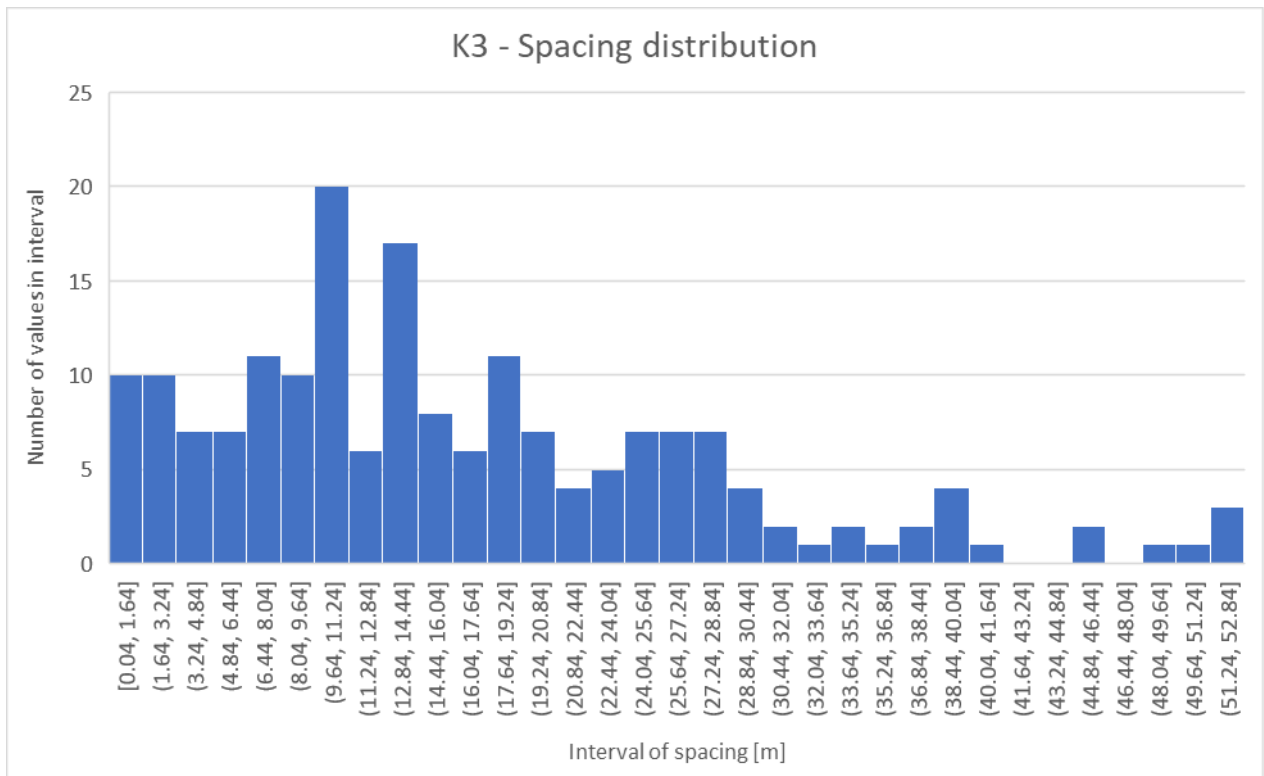


Figure 35: K3 - spacing distribution histogram

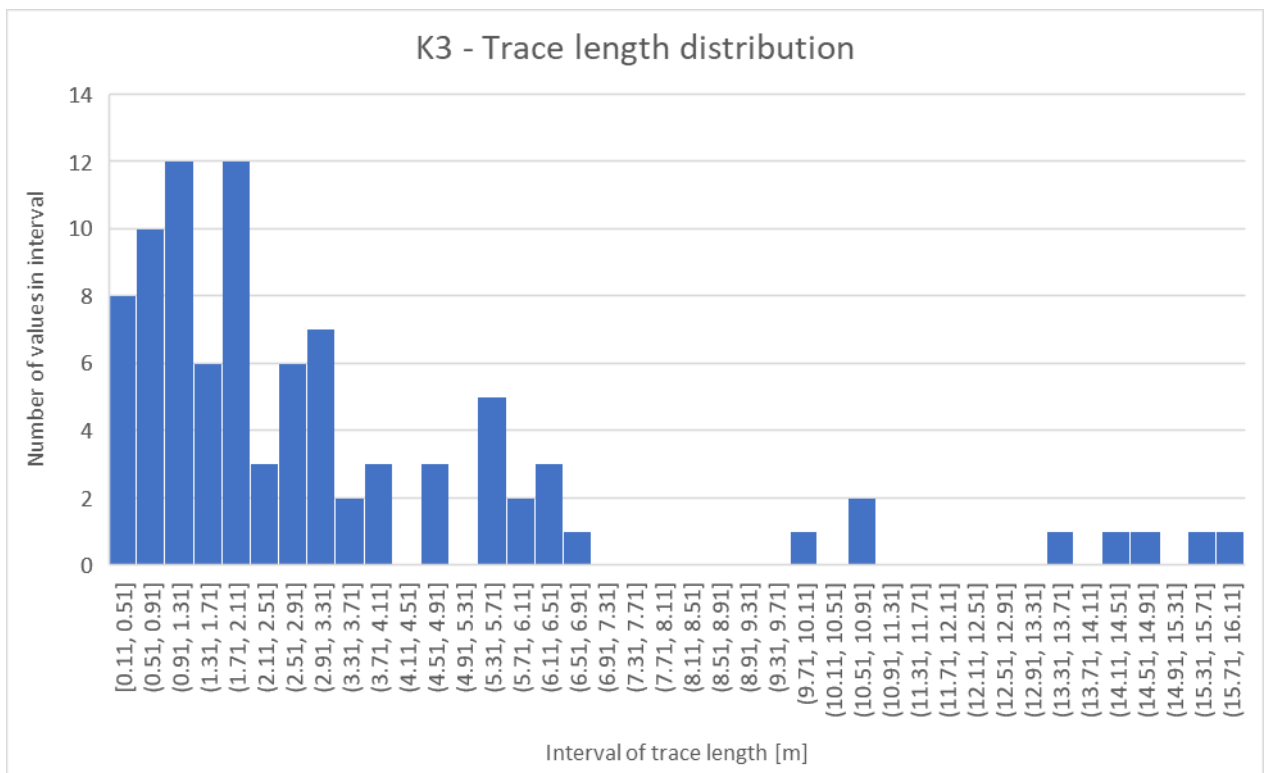


Figure 36: K3 - trace length distribution histogram